Impact of higher harmonics in searching for gravitational waves from nonspinning binary black holes

Collin Capano, Yi Pan, and Alessandra Buonanno

Maryland Center for Fundamental Physics and Joint Space Science Institute, Department of Physics, University of Maryland, College Park, Maryland 20742, USA

(Received 7 November 2013; published 20 May 2014)

Current searches for gravitational waves from coalescing binary black holes (BBH) use templates that only include the dominant harmonic. In this study we use effective-one-body multipolar waveforms calibrated to numerical-relativity simulations to quantify the effect of neglecting subdominant harmonics on the sensitivity of searches. We consider both signal-to-noise ratio (SNR) and the signal-based vetoes that are used to reweight SNR. We find that neglecting subdominant modes when searching for nonspinning BBHs with component masses $3\ M_\odot \leq m_1$, $m_2 \leq 200\ M_\odot$ and total mass $M < 360\ M_\odot$ in advanced LIGO results in a negligible reduction of the reweighted SNR at detection thresholds. Subdominant modes therefore have no effect on the detection rates predicted for advanced LIGO. Furthermore, we find that if subdominant modes are included in templates the sensitivity of the search becomes *worse* if we use current search priors, due to an increase in false alarm probability. Templates would need to be weighted differently than what is currently done to compensate for the increase in false alarms. If we split the template bank such that subdominant modes are only used when $M \gtrsim 100\ M_\odot$ and mass ratio $q \gtrsim 4$, we find that the sensitivity does improve for these intermediate mass-ratio BBHs, but the sensitive volume associated with these systems is still small compared to equal-mass systems. Using subdominant modes is therefore unlikely to substantially increase the probability of detecting gravitational waves from nonspinning BBH signals unless there is a relatively large population of intermediate mass-ratio BBHs in the universe.

DOI: 10.1103/PhysRevD.89.102003 PACS numbers: 04.30.-w, 04.80.Nn, 04.30.Db, 04.30.Tv

I. INTRODUCTION

Within the next few years the next generation of gravitational-wave detectors will come online. These detectors—the advanced Laser Interferometer Gravitational-wave Observatory (aLIGO) in the United States [1], the French-Italian Virgo observatory [2], the KAGRA detector in Japan [3], and a potential third LIGO detector in India [4]—will be sensitive to sources up to 10 times more distant than first generation detectors. One of the most promising sources of gravitational waves for these detectors are coalescing binary black holes (BBHs). As the two black holes in a binary orbit each other, they emit gravitational radiation; this causes them to inspiral and eventually merge into a single black hole. Advanced detectors will be able to detect radiation emitted during this process up to tens of Gpc away. The rate of BBH coalescences with masses detectable by the advanced detectors is highly uncertain: the detection rate has been estimated to be as low as $0.4\ \mathrm{yr}^{-1}$, but it may be as high as $1000\ \mathrm{yr}^{-1}$ [5]. If the optimistic end of this range is correct, BBHs would be the most prolific source of gravitational-wave detections in the advanced detector era.

Searches for BBHs use a matched filter to determine when a gravitational wave is likely to be present in a detector's data [6,7].[1] The filter produces a signal-to-noise ratio (SNR) that is proportional to the probability that a signal exists in the data with similar parameters as the template used in the correlation [10]. Since the physical parameters of the signal are unknown *a priori*, a discrete *bank* of templates is used to cover the range of possible parameters [11,12]. This technique for searching for gravitational waves relies on good agreement between templates and real signals. If there is significant disagreement between the two, the SNR will be reduced, and it becomes difficult to separate potential signals from noise. It is therefore important to verify that templates adequately resemble potential gravitational-wave signals.

Gravitational waveforms are decomposed into a -2 spin-weighted spherical harmonic basis ${}_{-2}Y_{lm}(\theta,\phi)$. Template waveforms used in past searches for BBHs have only

[1]Unmodeled "burst" searches [8] are also sensitive to BBHs [9]. Previously, these searches have been used to search for signals with total masses $M > 100\ M_\odot$, as the signals in this mass range did not have many cycles in the sensitive band of the initial generation of LIGO detectors. In this paper, we will consider signals with M as large as $360\ M_\odot$. Due to the improved low-frequency (< 40 Hz) sensitivity of the advanced detectors, template-based searches similar to those done in [6,7] will be feasible at these higher masses. We therefore only consider template-based searches here.

included the most dominant mode, $l = |m| = 2$ [6,7]. In addition, predictions of the number of detections that will be made in advanced LIGO have been made assuming both templates and signals only have the dominant mode [5]. Real signals, however, will have all modes. There can be significant *mismatch* [defined as $1 - \mathcal{E}$, where $\mathcal{E}$ is given by Eq. (13); see Sec. II C 1 for details] between waveforms that include subdominant modes and waveforms that only include the dominant mode [13–16]. This raises the question, by neglecting subdominant modes has the sensitivity of BBH searches been overstated? Furthermore, would sensitivity improve if templates included subdominant modes?

Several studies have investigated the effects of subdominant modes to try to answer these questions. The authors of Ref. [14] used waveforms generated from numerical relativity as both template and signal to measure mismatch when subdominant modes are not included in templates. They considered systems with total mass $M > 100\ \mathrm{M}_\odot$ and mass ratios $1 \leq q \leq 4$.[2] When computing overlaps they only considered templates which had the same intrinsic parameters (mass and spin) as signals. They found that adding subdominant modes could improve detection volume by up to 30%, but they noted that the largest gain in volume occurred for signals for which the detectors had the least sensitivity (these were systems with asymmetric masses and inclination angle—the angle between the orbital angular momentum and the line of sight to the detector—$\theta \approx \pi/2$).

To fully understand the effect of subdominant modes on the sensitivity of BBH searches, a bank of template waveforms covering the source parameter space is necessary. These waveforms should contain the complete inspiral, merger and ringodwn stages of subdominant modes since the latter become relatively stronger during the last stage of inspiral and merger. Here we employ effective-one-body (EOB) waveforms [17,18] calibrated to numerical-relativity simulations [13].

Building on an initial attempt [19] to calibrate subdominant modes, the authors of Ref. [13] built a nonspinning EOB model that includes four subdominant modes, namely the $(l, m) = (2, 1), (3, 3), (4, 4)$ and $(5, 5)$ modes, as well as the dominant $(l, m) = (2, 2)$ mode. The EOB model of Ref. [13] was calibrated to numerical-relativity simulations of mass ratios $q \leq 6$.[3] A direct study [21] carried out with the Markov chain Monte Carlo technique demonstrated that the EOB waveforms of Ref. [13] are indistinguishable from the numerical-relativity waveforms [22] used to calibrate them up to SNR $= 50$ for the advanced LIGO detectors. Furthermore, preliminary studies in Ref. [13] suggested that the EOB waveforms containing subdominat modes could be sufficiently accurate to search for nonspinning BBH signals of $q \leq 6$, at least in the relatively narrow frequency band where direct comparison with numerical-relativity waveforms was possible. The recent investigation of Ref. [23] verified the accuracy of these EOB waveforms in the entire sensitivity band of advanced LIGO detectors. Having the correct limit for $q \to \infty$ by construction, we expect EOB waveforms to be reasonably accurate when $q > 6$. This expectation was recently reinforced by the excellent agreement found against a $q = 10$ numerical-relativity waveform [24]. Finally, the dominant mode EOB waveforms that we use here have been employed as simulated signals in the most recent LIGO BBH searches [7].

Using a bank of dominant-mode templates that allows maximization over the masses of the binaries, Ref. [15] studied templates and signals with component masses $3\ \mathrm{M}_\odot \leq m_1, m_2 \leq 25\ \mathrm{M}_\odot$. They also found that subdominant modes had little effect on equal-mass systems, but argued that sensitive volume could be increased by as much as 25% for systems with $q \geq 4$ and inclination angles $1.08\ \mathrm{rad} \leq \theta \leq 2.02\ \mathrm{rad}$ if subdominant modes were added to templates.

Both of these studies calculated what percentage of sensitive volume could be gained if subdominant modes were added to templates by finding the fractional loss in SNR of signals with subdominant modes when they were recovered by dominant-mode templates. However, estimating the gain in sensitive volume in this manner neglects additional complications that arise when searching in real, non-Gaussian, data. In real data a signal-based veto, χ^2 [25], is used to reweight SNR [6,7]. *Reweighted SNR* is needed in order to separate potential gravitational-wave signals from non-Gaussian transients that are present in detector data [26]. Any mismatch between the templates and signals causes an increase in χ^2, which in turn causes a decrease in reweighted SNR relative to SNR. Thus the sensitivity of dominant-mode templates to real signals may be worse than predicted from SNR considerations alone. This makes the case for adding subdominant modes to templates stronger.

A signal must have high statistical significance in order for it to be considered a gravitational-wave candidate. The standard measurement of significance is *false-alarm probability*, which is the probability that an event caused by noise is misidentified as a signal. When calculating sensitive volume, the SNR threshold is chosen such that the false-alarm probability at that threshold is small. In Refs. [14] and [15] the same SNR threshold was used when estimating the sensitive volume of dominant-mode templates and the potential sensitive volume of subdominant mode templates. Both studies acknowledged that adding subdominant modes to templates can increase the probability of getting a false alarm. To keep the false-alarm

[2]In this paper we use the convention that $q = m_1/m_2$ with $m_1 \geq m_2$.

[3]An EOB model with slightly different parametrization was calibrated to the same set of numerical-relativity waveforms and provides two subdominant modes $(l, m) = (2, 1)$ and $(3, 3)$ [20].

probability fixed, the SNR threshold in a search that uses subdominant mode templates must therefore increase. This increase in threshold decreases the sensitive volume that can be obtained by subdominant mode templates, making the case for adding subdominant modes to templates weaker.

Due to these conflicting factors it is difficult to make a definitive statement about the impact of subdominant modes on BBH searches from SNR considerations alone. In this paper we resolve the uncertainty by finding both SNR and χ^2 between templates without subdominant modes and signals with subdominant modes. Doing so, we are able to estimate the fraction of sensitive volume that is lost by neglecting subdominant modes when reweighted SNR is used. We also simulate a search with subdominant modes: we estimate the increase in threshold needed to keep the false-alarm probability fixed, thereby allowing an accurate comparison of search volumes when subdominant modes are included and excluded in templates. We consider nonspinning BBHs with component-masses $3\ \mathrm{M}_\odot \leq m_1$, $m_2 \leq 200\ \mathrm{M}_\odot$ and with total mass $M < 360\ \mathrm{M}_\odot$. We therefore cover the entire range of "stellar-mass" BBHs that were searched for in LIGO and Virgo data in the past ($m_1, m_2 \in [3, 97]\ \mathrm{M}_\odot$; $M \leq 100\ \mathrm{M}_\odot$) [7,27], and we cover binaries that involve "intermediate-mass black holes" which may form from dynamical capture in globular clusters [28]. To generate both dominant-mode and subdominant mode waveforms we use the EOB model calibrated to numerical-relativity simulations, as obtained in Ref. [13].

For simplicity, and as was done in Refs. [14,15], we study the effect of subdominant modes using a single detector (real searches use a network of detectors). We simulate an advanced LIGO detector by generating stationary Gaussian noise colored by the zero-detuned, high-power advanced LIGO design curve [29]. Due to the presence of non-Gaussian transients there is currently no model for the noise distribution of real detector data [30,31]. However, by injecting signals into Gaussian noise we find the best sensitivity that can be obtained by the search. We reason that if subdominant mode templates have worse sensitivity than dominant-mode templates in Gaussian noise, those templates will fare no better in real detector data. Furthermore, current detection pipelines are able to mitigate noise transients such that the sensitive volumes of real detectors are within a factor of a few of what they would be if the data were Gaussian [26]. The sensitive volumes we find using Gaussian noise is thus a good approximation of what they will be in real detector data (assuming advanced detectors have similar data-quality characteristics).

In this paper we are concerned primarily with the effects of subdominant modes on our ability to *detect* gravitational waves; we do not address the effect on *parameter estimation*. The goal of detection is to determine whether or not a signal exists in some data, regardless of the parameters. When doing parameter estimation, on the other hand, a signal is assumed to be in the data; the goal is then to find the best fitting parameters.[4] These differing goals put different constraints on what to use as template waveforms. As we will see, including subdominant modes in templates does not improve our ability to detect if the subdominant modes do not increase the SNR of signals enough to offset increases in false-alarm probability. If a signal is assumed to be present, however, then adding subdominant modes to template waveforms can only improve parameter estimation if the resulting waveform is a better match to the signal. Indeed, it has been shown [16,21] that including subdominant modes reduces systematic bias when measuring the parameters of signals.

The rest of this paper is divided as follows. Section II provides background for the search methods and statistics we discuss. In Sec. II A we review how SNR is calculated using dominant-mode templates. In Sec. II B we review the χ^2 statistic and how it is used to reweight the SNR. In Sec. II C we discuss the statistics we use in this paper to compare the sensitivity of searches. In Sec. II D we provide a brief review of the astrophysics of BBHs to motivate our choice of masses and rate priors. We show that the bank of dominant-mode templates we use is effectual to dominant-mode signals across the mass space we investigate in Sec. III A. In Sec. III B we find the sensitivity of this bank to signals with subdominant modes to see if subdominant modes have an effect on predicted sensitivity. In Sec. IV we estimate the sensitivity of a simulated bank of subdominant mode templates using equations derived in Appendixes B and A. Finally, in Sec. V we review and discuss our results.

II. REVIEW OF CURRENT SEARCHES AND TEMPLATE MODELING

The strain induced in a detector from a passing gravitational wave is [33]

$$h(t;\boldsymbol{\Upsilon},\boldsymbol{\Xi}) = \frac{1}{r}(F_+(\alpha,\delta,\psi)h_+(t-t_c;\theta,\phi,\phi_0,\boldsymbol{\Upsilon}) + F_\times(\alpha,\delta,\psi)h_\times(t-t_c;\theta,\phi,\phi_0,\boldsymbol{\Upsilon})), \quad (1)$$

where

$$h_{(+,\times)} = (\Re,\Im)\sum_{lm} {}_{-2}Y_{lm}(\theta,\phi)A_{lm}(t-t_c;\boldsymbol{\Upsilon}) \times \exp\left[-i(\Psi_{lm}(t-t_c;\boldsymbol{\Upsilon}) + m\phi_0)\right]. \quad (2)$$

Here, ${}_{-2}Y_{lm}(\theta,\phi)$ are the -2 spin-weighted spherical harmonics, r is the distance to the source from the detector,

[4] In prior searches, a detection pipeline was run on data first to identify times when candidate signals exist; these times were then followed up by parameter estimation pipelines [32].

ϕ_0 is the initial phase of the binary, and t_c is the coalescence time of the binary. The angle θ is the angle between the orbital-angular momentum and the line-of-sight to the detector (the *inclination*); ϕ is the azimuthal angle to the projection of the line-of-sight on to the orbital plane. The functions F_+ and $F_\times$ project the gravitational wave from the source's radiation frame into the detector's frame; they are functions of the right ascension (α), declination (δ), and polarization (ψ) of the source with respect to the detector [34].[5] Since we only consider nonspinning waveforms in this paper, the *intrinsic* parameters $\boldsymbol{\Upsilon}$ are the component masses m_1 and m_2. Neglecting spin also means that ϕ and ϕ_0 are degenerate, and we can set $\phi_0 = 0$. Together the parameters $\{t_c, r, \theta, \phi, \alpha, \delta, \psi\}$ make up the *extrinsic* parameters $\boldsymbol{\Xi}$.

A. SNR maximization for a dominant mode bank

Given some detector data s we wish to determine whether or not a gravitational-wave signal h is present in it. We do not know *a priori* the parameters of h. In order to maximize the probability of detection we must therefore search over all possible intrinsic and extrinsic parameters that h may have. To do this, we calculate the signal-to-noise ρ maximized over $\boldsymbol{\Upsilon}$ and $\boldsymbol{\Xi}$:

$$\rho = \max_{\boldsymbol{\Upsilon},\boldsymbol{\Xi}} \frac{\langle h(t;\boldsymbol{\Upsilon},\boldsymbol{\Xi}), s(t)\rangle}{\sqrt{\langle h(t;\boldsymbol{\Upsilon},\boldsymbol{\Xi}), h(t;\boldsymbol{\Upsilon},\boldsymbol{\Xi})\rangle}}. \tag{3}$$

The inner product $\langle \cdot, \cdot \rangle$ is defined as [35]

$$\langle a, b\rangle = 4\Re \int_0^\infty \frac{\tilde{a}^*(f)\tilde{b}(f)}{S_n(f)} \mathrm{d}f, \tag{4}$$

where $S_n(f)$ is the one-sided power spectral density (PSD) of the noise. In this paper we use the zero-detuned, high-power, advanced LIGO design curve [29]. This PSD grows substantially at frequencies below ~10 Hz due to seismic noise. As was done in Ref. [15], we use a lower frequency cutoff of 15 Hz for our matched filter. We terminate the filter at a frequency larger than the ringdown frequency of the signal.

In principle we must maximize the SNR over 8 parameters for nonspinning systems—2 intrinsic plus 6 extrinsic[6]—but this number can be reduced. Let

$$|F| = \sqrt{F_+^2 + F_\times^2}, \tag{5}$$

$$\kappa = \arctan\left(\frac{F_\times}{F_+}\right); \tag{6}$$

then

$$h = \frac{1}{\mathcal{D}}(h_+ \cos\kappa + h_\times \sin\kappa), \tag{7}$$

where $\mathcal{D} = |F|/r$ is the *effective distance* [35]. Since $\mathcal{D}$ cancels in the SNR, we need not maximize over it. We can thus maximize over α, δ, and ψ by simply maximizing κ.

The coalescence time is maximized over by evaluating the SNR at discrete time intervals, selecting points where ρ is at a maximum and exceeds some threshold. These points are *triggers*. In Ref. [35] it is shown that $\rho(t)$ can be efficiently calculated by taking the inverse Fourier transform of $\tilde{h}^*(f)\tilde{s}(f)/S_n(f)$. Since we are interested in the effect of subdominant modes, which do not affect the maximization over coalescence time, we will make this maximization implicit and set $t_c = 0$ throughout the rest of this paper.

In order to maximize over the intrinsic parameters a template bank is used [11,12]. Templates are typically laid out across the search parameter space such that no more than 3% of the SNR is lost due to the discreetness of the bank [6,7]. The SNR is maximized over the extrinsic parameters for each trigger; the template with the largest SNR is then selected, thereby maximizing over the intrinsic parameters.

With these considerations Eq. (3) simplifies to

$$\rho = \max_{\theta,\phi,\kappa} \frac{\langle h_+(t;\theta,\phi), s(t)\rangle \cos\kappa + \langle h_\times(t;\theta,\phi), s(t)\rangle \sin\kappa}{\sqrt{\langle h(t;\kappa,\theta,\phi), h(t;\kappa,\theta,\phi)\rangle}}. \tag{8}$$

If the templates contain subdominant modes, then the number of parameters that need to be maximized over can be reduced no further. In Appendix A we perform the maximization over κ analytically when subdominant modes are included (the maximization over θ and ϕ must be done numerically). This is used to model a hypothetical search using subdominant modes, which is discussed in Sec. IV. In current searches, template waveforms are generated using only the dominant, $l = |m| = 2$, mode. In that case θ, ϕ, and κ are all degenerate with each other and the maximization reduces to a single parameter. This can be performed analytically, yielding [10]

$$\rho = \sqrt{\frac{\langle h_+(t), s(t)\rangle^2 + \langle h_\times(t), s(t)\rangle^2}{\langle h, h\rangle}}. \tag{9}$$

In stationary Gaussian noise containing no signal, ρ is χ distributed (or equivalently, ρ^2 is χ^2 distributed) with two degrees of freedom.

[5]Due to the motion of the Earth, F_+ and $F_\times$ are also functions of time. Here we assume that the relative displacement of the detector is small across the duration of the signal in the detector's band.

[6]We do not need to maximize over r since it cancels in the SNR.

B. The χ^2 test and reweighted SNR

Real data from the LIGO and Virgo detectors contain a number of non-Gaussian transients (*glitches*) [30,31]. To mitigate the effect of these glitches the χ^2 statistic is calculated to better separate noise from potential signals. This is calculated as follows: split the matched filter into p frequency bins such that the template has equal amounts of power in each bin, and let ρ_i be the SNR of a trigger in the ith bin. If the signal matches the template then $\rho_i \approx \rho/p$. We can therefore quantify how well a signal matches a template by defining [25]

$$\chi^2 = p\sum_{i=1}^{p}\left|\rho_i - \frac{\rho}{p}\right|^2. \tag{10}$$

If the template matches the signal exactly then the χ^2 statistic will be χ^2 distributed with $2p-2$ degrees of freedom (hence the name). If there is any mismatch between the signal and the template, the mean χ^2 is [25]

$$\langle\chi^2\rangle = 2p - 2 + \mu^2\rho^2, \tag{11}$$

where μ is a measure of the mismatch. Thus the larger the mismatch between the signal and the template, the larger the χ^2 statistic. Since the increase in χ^2 is proportional to ρ, even "loud" (large SNR) glitches are mitigated by χ^2 as they will have high mismatch to the template.

In BBH searches χ^2 is used to reweight ρ, obtaining the *reweighted SNR* $\tilde{\rho}$.[7] As it is based on characteristics of the data and the templates, the exact form of the weighting evolved throughout the initial LIGO era. Generally, the weighting is such that ρ is reduced for triggers with high χ^2. In this study we use the reweighted SNR that was used in the most recent searches [6,7], which is defined as[8]

$$\tilde{\rho} = \begin{cases} \rho & \text{for } \chi_r^2 \le 1, \\ \rho[\frac{1}{2}(1+(\chi_r^2)^3)]^{-1/6}, & \text{for } \chi_r^2 > 1, \end{cases} \tag{12}$$

where χ_r^2 is the *reduced* χ^2, which is χ^2 divided by the number of degrees of freedom.

Reweighting the SNR using χ^2 is crucial to BBH searches. A SNR of 8 is typically used when predicting detection rates [5], but it would not be possible to detect at this ρ without some type of χ^2 reweighting of glitches [26]. However, if signals also significantly mismatch the templates then the use of $\tilde{\rho}$ can adversely affect the efficiency to these signals. The effect on efficiency from the mismatch between signals and templates therefore cannot be determined from the loss in SNR alone. For this reason, in the following sections we investigate the effect on χ^2 due to the mismatch between dominant-mode templates and signals with subdominant modes, and we calculate efficiency using $\tilde{\rho}$.

C. Quantifying the ability of a search to make detections

The purpose of our study is to investigate whether adding subdominant modes to templates will improve our ability to detect gravitational waves from nonspinning BBHs. Ultimately, we want to know what template bank maximizes the number of detections made per unit time. To do so we need to quantify the ability of a bank with dominant-mode templates and a bank of templates with subdominant modes to recover waveforms with subdominant modes. For this purpose we calculate *effectualness*; we also calculate *efficiency*, from which we find *sensitive volume* and *relative gain*.

1. Effectualness

Effectualness[9] is a statistic that is commonly used to quantify how well one family of waveforms recovers another. Given a simulated signal $h^\dagger$ with parameters $\mathbf{\Theta} = (\mathbf{\Upsilon}, \mathbf{\Xi})$ and a bank of templates $\{h(\mathbf{\Theta}')\}$, effectualness is defined as [36,37]

$$\mathcal{E}_{ab}(\mathbf{\Theta}) = \max_{\mathbf{\Theta}'} \frac{\langle h_a(\mathbf{\Theta}'), h_b^\dagger(\mathbf{\Theta})\rangle}{\sqrt{\langle h_a(\mathbf{\Theta}'), h_a(\mathbf{\Theta}')\rangle\langle h_b^\dagger(\mathbf{\Theta}), h_b^\dagger(\mathbf{\Theta})\rangle}}. \tag{13}$$

Here and elsewhere we adopt subscripts on $\mathcal{E}$ to indicate whether or not the signal and templates have subdominant modes; the first index indicates the templates, the second the signal. We will use S to indicate a waveform that has subdominant modes and D to indicate a waveform without subdominant modes. For example, $\mathcal{E}_{\mathrm{DS}}(\mathbf{\Theta})$ is the effectualness of a bank of templates without subdominant modes to a signal with subdominant modes and parameters $\mathbf{\Theta}$.

If a signal $h^\dagger$ is in stationary Gaussian noise with zero mean, the expectation value of the overlap with a template h is $\langle h, s = h^\dagger + n\rangle = \langle h, h^\dagger\rangle$. The maximum overlap occurs when h and $h^\dagger$ have the same parameters and come from the same waveform model. Thus, via Eq. (3), the expectation value of the maximum recoverable SNR of a signal $h^\dagger$ is

$$\max\langle\rho\rangle = \sqrt{\langle h^\dagger, h^\dagger\rangle}. \tag{14}$$

Effectualness therefore gives the fraction of available SNR in a signal $h_b^\dagger$ that is recovered by the template h_a:

[7] A cut on large χ^2 values is also employed, but this cut is chosen conservatively in order to not remove any signals [26]. As such, it is mostly used to reduce the number of triggers for computational purposes. We therefore do not consider it here.

[8] In Ref. [7], a different weight than that given in Eq. (12) was used for triggers whose templates had duration < 0.2 s. All of the templates in our study have durations > 1 s, however, due to the better low-frequency performance of the advanced LIGO noise curve we use. We therefore use Eq. (12) for all triggers.

[9] Effectualness has also been referred to as "fitting factor" [36].

$$\mathcal{E}_{ab}(\mathbf{\Theta}) = \frac{\langle \rho_{ab}(\mathbf{\Theta})\rangle}{\max \langle \rho_{bb}(\mathbf{\Theta})\rangle}. \tag{15}$$

Here, $\langle \rho_{ab}(\mathbf{\Theta})\rangle$ indicates the expectation value of the SNR of signal $h_b^\dagger(\mathbf{\Theta})$ using templates $\{h_a(\mathbf{\Theta}')\}$.[10] The smaller the effectualness, the less SNR recovered by the template and the closer signals need to be in order to detect them. Effectualness is thus an estimate of how sensitive a bank of templates will be to a particular set of signals.

However, effectualness is not sufficient for comparing the sensitivity of a set of templates to signals created with different waveform models. We see from Eq. (15) that a drop in effectualness can result from a decrease in the overlap between two waveforms or from an increase in the maximum recoverable SNR. This ambiguity has particular relevance for subdominant modes. The predicted detection rates of advanced LIGO are made assuming that both signals and templates have the dominant mode only [5]. Real signals will have subdominant modes. If $\mathcal{E}_{\rm DS} < \mathcal{E}_{\rm DD}$ for some signals, it is not clear from effectualness alone whether the loss is due to $\langle \rho_{\rm DS}\rangle < \langle \rho_{\rm DD}\rangle$ or if it is because $\max\langle \rho_{\rm SS}\rangle > \max\langle \rho_{\rm DD}\rangle$. If entirely the first case, detection rates will be less than predicted. If entirely the second case, the sensitivity of aLIGO will be the same as predicted (perhaps better, since the additional power in the subdominant modes may give larger SNR than expected). The drop in effectualness in this case only indicates that the sensitivity could be better than predicted if subdominant modes were added to templates, but it will not be worse.

It is also not clear what effect a decrease in effectualness has on reweighted SNR. Equation (11) indicates that larger mismatch between signal and template results in larger χ^2; this increase results in lower $\tilde{\rho}$. Since reweighted SNR is used as the ranking statistic in real searches, the decrease in effectualness (increase in mismatch) may result in a further reduction in sensitivity via χ^2.

Finally, effectualness implicitly assumes that SNR is the optimal statistic (in the Neyman-Pearson sense) to detect a gravitational wave in Gaussian noise. While this has been shown to be true when the intrinsic parameters of the signal are known [10], it is not necessarily true if the intrinsic parameters are unknown, as is the case in real BBH searches. Finding the optimal statistic in this case is difficult to do, as the waveforms have a nontrivial dependence on the intrinsic parameters. Moreover, we would need to know the distribution of the sources' intrinsic parameters, which in our case are the masses of BBHs. As we will see in Sec. II D the mass distribution of BBHs is highly uncertain. Even if we could find the optimal statistic for an assumed distribution, the statistic may not be optimal for the real astrophysical distribution.

In practice, we get around these difficulties by simply assuming that SNR maximized over the template bank is a good approximation to the optimal statistic. In doing so, we assume that each template is equally likely to detect a signal, which implicitly assumes a particular astrophysical distribution. Effectualness then gives us a measure of the performance of the bank assuming that distribution is correct. However, if the implicit distribution is not correct, then SNR maximized over the bank is not a good approximation of the optimal statistic, thereby making effectualness a poor metric for search sensitivity.

For these reasons the effect of subdominant modes on the sensitivity of a search cannot be ascertained by effectualness alone. A more informative metric is the sensitive volume, which is found from efficiency.

2. Efficiency, sensitive volume, and relative gain

Given a set of N simulated signals with intrinsic and extrinsic parameters $\mathbf{\Theta}$ and generated from waveform-model b, $\{h_b^\dagger(\mathbf{\Theta})\}$, the efficiency of a bank of templates generated from waveform-model a is the fraction of signals found with $\tilde{\rho}$ larger than some threshold value at a distance r [38]; i.e.,

$$\epsilon_{ab}(r, \mathbf{\Upsilon}) = \frac{n_{ab}(r, \mathbf{\Upsilon})}{N_b(r, \mathbf{\Upsilon})}. \tag{16}$$

As with effectualness subscripts indicate the type of waveform used for the templates and signals; e.g., $\epsilon_{\rm DS}$ is the efficiency of a dominant mode bank to subdominant mode signals. Note that, aside from r, ϵ_{ab} is a function of the intrinsic parameters only ($\mathbf{\Upsilon}$). Since the universe is isotropic at the distances we are considering, the rest of the extrinsic parameters are accounted for by uniformly distributing signals in $\{\theta, \phi, \phi_0, \alpha, \delta, \psi\}$.

When determining efficiency in real searches the threshold $\tilde{\rho}$ is determined by the loudest event in the data [6,7]. In this study we use $\tilde{\rho} = 8$ as the threshold. SNR (ρ) equal to 8 is commonly used as a threshold for predicting detection rates [5]. For well-matched signals, $\tilde{\rho} \approx \rho$ when $\rho = 8$; using $\tilde{\rho} = 8$ as a threshold should therefore give roughly the same results as predictions if mismatches between signals and templates are not too large.

The expected rate of gravitational-wave detections per unit time is

$$\mathcal{R}_{\rm detect} = \int \epsilon(r, \mathbf{\Upsilon}) R(V, \mathbf{\Upsilon}) \mathrm{d}V \mathrm{d}\mathbf{\Upsilon}, \tag{17}$$

where $R(V, \mathbf{\Upsilon})$ is the average rate of coalescing BBHs with intrinsic parameters $\mathbf{\Upsilon}$ in volume V. Assuming $R(V, \mathbf{\Upsilon})$ is constant over volumes for which $\epsilon \neq 0$ and uniform in a small region in parameter space $\mathbf{\Upsilon} + \Delta\mathbf{\Upsilon}$, we define the sensitive volume V_{ab} as

[10]Note that $\max \langle \rho_{bb}(\mathbf{\Theta})\rangle$ is not the same as $\langle \rho_{bb}(\mathbf{\Theta})\rangle$. This is because $\langle \rho_{bb}(\mathbf{\Theta})\rangle$ indicates the SNR of a bank of templates $\{h_b(\mathbf{\Theta}')\}$ to a signal $h_b^\dagger(\mathbf{\Theta})$. In fact, while the waveform models may be the same, the template and signal parameters may not be due to the discreetness of the bank.

$$V_{ab}(\boldsymbol{\Upsilon}+\Delta\boldsymbol{\Upsilon}) = 4\pi \int_0^\infty \epsilon_{ab}(r,\boldsymbol{\Upsilon}+\Delta\boldsymbol{\Upsilon}) r^2 \mathrm{d}r. \quad (18)$$

With these assumptions, V_{ab} is proportional to the average rate of detections in $\boldsymbol{\Upsilon}+\Delta\boldsymbol{\Upsilon}$.

We assume that all of the error in the sensitive volume is due to error in the measurement of the efficiency from statistical fluctuations in the noise. This error is derived from the range of efficiency values for which the number of found injections varies no more than one standard deviation [39]:

$$(n-\langle n\rangle)^2 \leq \langle n^2\rangle - \langle n\rangle^2.$$

The mean and variance are given by the binomial distribution:

$$\langle n\rangle = N\epsilon,$$
$$\langle n^2\rangle = N\epsilon(1-\epsilon).$$

Using these values and solving for ϵ yields [39]

$$\pm\delta\epsilon_i = \frac{N_i(2n_i+1) \pm \sqrt{4N_i n_i(N_i-n_i)+N_i^2}}{2N_i(N_i+1)}, \quad (19)$$

where the index i indicates the efficiency and number of injections in the ith distance bin (dependence on waveforms a, b and parameters $\boldsymbol{\Upsilon}$ made implicit). This error is then propagated to the volume via Eq. (18). Note that this results in a conservative estimate of δV. In our study we average over several realizations of noise when finding $\tilde{\rho}$; thus actual statistical fluctuations in ϵ_{ab} are less than what is assumed in Eq. (19).

To compare the sensitivity of two template banks to a set of simulated signals we define the relative gain $\mathcal{G}^{cd}_{ab}$,

$$\mathcal{G}^{cd}_{ab}(\boldsymbol{\Upsilon}+\Delta\boldsymbol{\Upsilon}) = \frac{V_{cd}(\boldsymbol{\Upsilon}+\Delta\boldsymbol{\Upsilon})}{V_{ab}(\boldsymbol{\Upsilon}+\Delta\boldsymbol{\Upsilon})}. \quad (20)$$

The upper (lower) indices denote the waveform models used for templates and signals in the numerator (denominator). Since sensitive volume is proportional to the detection rate, the relative gain gives the average number of detections per unit time the cd search will make relative to the ab search.

D. Astrophysical priors on the distribution of BBH masses

When comparing the sensitivity of template banks it can happen that one bank has better sensitivity in one area of parameter space, but worse sensitivity in another. We will see this in Sec. IV; templates with subdominant modes have better sensitivity at $M > 100\ \mathrm{M}_\odot$ and $q \gtrsim 10$, but worse sensitivity for lower mass and more equal-mass systems. This raises the question of whether the gain in sensitivity in one area of parameter space is large enough to offset the loss in another. In this case it is useful to try to find the *net* relative gain, which is

$$\mathrm{net}\{\mathcal{G}^{cd}_{ab}\} = \frac{\int R(\boldsymbol{\Upsilon}) V_{cd}(\boldsymbol{\Upsilon}) \mathrm{d}\boldsymbol{\Upsilon}}{\int R(\boldsymbol{\Upsilon}) V_{ab}(\boldsymbol{\Upsilon}) \mathrm{d}\boldsymbol{\Upsilon}}. \quad (21)$$

Doing so gives the relative number of detections made over the entire parameter space; if the net gain is > 1 the gain in sensitivity in one area of parameter space is worth the loss in another.

Calculating net gain requires knowledge of the rate of BBH coalescence, $R(\boldsymbol{\Upsilon})$. Unfortunately, this is highly uncertain. For a BBH with $m_1 = m_2 = 10\ \mathrm{M}_\odot$, the coalescence rate has been estimated to be anywhere from $O(10^{-4})$ to $O(10^{-1})\ \mathrm{Mpc}^{-3}\,\mathrm{Myr}^{-1}$, leading to predicted detection rates between 0.4 and 10^3 per year in advanced LIGO [5]. We do not need to know the magnitude of the BBH coalescence rate in order to calculate the net gain—we only need the relative distribution in mass—but even this is largely uncertain.

Binary black holes with masses detectable by LIGO are thought to be formed in one of two ways: via the two stars in an isolated binary each collapsing into black holes (*field binaries*), or by a black hole capturing another black hole in a dense stellar region such as globular clusters [40]. No BBHs have been directly observed; their existence is predicted from population synthesis models, from the predicted evolution of known x-ray binaries, and from considerations of the dynamics of black holes in dense stellar clusters [5].

The most massive black holes formed from stellar collapse known are in the x-ray binaries IC 10 X-1 and NGC 300 X-1 [41,42]. These black holes have been estimated to have masses between 20 and $35\ \mathrm{M}_\odot$, but population synthesis models predict that black holes formed from isolated field stars may have masses as large as $80\ \mathrm{M}_\odot$ in low-metallicity environments [43]. The mass distribution of black holes in field binaries are more difficult to predict, however, as the proximity of the two progenitor stars to each other add several complications [44]. Population synthesis models give varying results depending on the values assumed for input parameters, but models generally suggest field binaries have $M \lesssim 100\ \mathrm{M}_\odot$ [45], with the peak of the distribution occurring around $20\ \mathrm{M}_\odot$ (cf. Figs. 8 and 9 of Ref. [45]). The distribution in mass ratio is also uncertain: some models predict equal-mass systems are more likely, while others predict a roughly uniform distribution between $q = 1$ and 4 (cf. Fig. 9 of Ref. [44]).

Black holes formed from dynamical capture in globular clusters may have masses between 10^2 and $10^4\ \mathrm{M}_\odot$ [28]. The existence of these intermediate-mass black holes

(IMBHs) is more speculative but is supported by observations of ultraluminous x-ray sources [46]. If IMBHs do exist they may form binaries with other IMBHs or with stellar-mass black holes, thus forming BBHs with larger total masses and mass ratios than possible in field binaries [5]. The merger rate between an IMBH with mass between 50 and 350 $M_\odot$ and a stellar-mass black hole with mass m has been estimated to be $\sim(0.02/m)\ \mathrm{Mpc}^{-3}\,\mathrm{Myr}^{-1}$ [47]. This is an optimistic estimate [5], but if correct, the rate of these *intermediate-mass-ratio inspirals* (IMRIs) could be on the same order of magnitude as BBHs formed from field binaries.

In this paper we consider BBHs with $3 \leq m_1,\ m_2 \leq 200\ M_\odot$ and $M \leq 360\ M_\odot$. We therefore cover the entire predicted mass range of field binaries and the lower end of IMBH/IMBH and IMRI binaries. (Our choice of masses is based on the effectualness of the template placement algorithm we use; see Sec. III for details.) Due to the large uncertainty in mass distribution across this range, we will simply assume a uniform rate in m_1 and m_2 to calculate net gain. This choice of astrophysical prior weights equal-mass systems as being more likely to occur than asymmetric-mass systems. Since this may bias our results (subdominant modes are more significant in higher mass-ratio systems) we will also consider a rate uniform in M and q. We will find that BBHs with $M > 100\ M_\odot$ are the dominant contribution to the net gain using these rate priors, as the sensitive volumes of these larger mass systems can be 1–2 orders of magnitude larger than lower-mass BBHs. Since the existence of IMBHs is more speculative, we additionally report net gains when only stellar-mass BBHs ($M < 100\ M_\odot$) are considered.

The astrophysical rates we use are only meant to be rough approximations for comparisons between template banks; we do not attempt to calculate detection rates. We do, however, report sensitive volumes across the mass space [see Fig. 10]. If a particular astrophysical prior is chosen, our results can be used to estimate the total number of nonspinning BBH detections that will be made in advanced LIGO.

III. IMPACT OF SUBDOMINANT MODES ON A DOMINANT MODE TEMPLATE BANK

Past BBH searches have used waveforms without subdominant modes as templates [6,7]. Predicted advanced LIGO detection rates are also based on considerations of the dominant mode only [5]. This assumes that the effect of neglecting subdominant modes is small. To test the validity of this assumption we compare the sensitivity of a template bank without subdominant modes to simulated signals without subdominant modes and to signals with subdominant modes.

We generate one million simulated signals (*injections*) uniformly distributed in component mass, inclination, sky location, distance, and polarization. Component masses are between 3 and 200 $M_\odot$, resulting in total masses (M) between 6 and 400 $M_\odot$ and mass ratios (q) between 1 and ~66. Distance limits are chosen such that an optimally oriented signal with the same masses as a given injection would produce an SNR between 6 and 100. For each injection we generate a version without subdominant modes and a version with subdominant modes, both at the same physical distance, using the EOB waveform calibrated to numerical relativity that is described in Ref. [13].[11] Template waveforms are the dominant-mode version of this waveform.

To calculate the reweighted SNR of each injection we generate 16 realizations of Gaussian noise colored by the zero-detuned high power noise curve. We use a different set of 16 realizations for each injection. In each realization we calculate the maximum SNR before the injection is added to the noise and after. If the SNR with the injection in the noise is larger than the SNR from noise alone, we record the SNR and calculate χ^2 and reweighted SNR. We then find the mean ρ, χ^2, and $\tilde{\rho}$ to get a measure of their expectation values. Only realizations that produced an SNR louder than noise are included in the average.

Due to computational constraints we are not able to calculate reweighted SNR for every template for every injection. Instead, we use the best matching template from the effectualness study to calculate $\tilde{\rho}$. This is equivalent to maximizing on SNR, then finding reweighted SNR, which is what current searches do [26]. We note that maximizing on $\tilde{\rho}$ might give better sensitivity, but since this is not what is currently done we do not investigate this idea further.

To calculate the sensitive volume we create 16 bins uniformly distributed in M and 10 bins uniformly distributed in $\log q$, keeping bins which have at least 1000 injections in them. Within each mass bin we create 20 bins uniform in log distance. We find the efficiency in each distance bin, then numerically integrate over the distance bins to get the sensitive volume. The distance bins span the smallest injected distance to the largest within the given mass bin. For distances smaller then the closest injection we assume $\epsilon = 1$; for distances larger than the furthest injection we assume $\epsilon = 0$.

A. Effectualness of the dominant-mode bank

Past BBH searches [6,7] have constructed template banks by placing templates in parameter space such that no more than 3% of SNR is lost due to the discreetness of the bank. In other words, templates are placed such that the *minimal match*, which is the minimum of the effectualness of the bank, is $\geq 97\%$. Templates are placed in a hexagonal grid [49] using a metric calculated from the mismatch

[11]Specifically, we use the EOBNRv2 code in the LSC Algorithm Library (LAL) [48] to generate dominant-mode waveforms. For subdominant mode waveforms we use the EOBNRv2HM code in LAL.

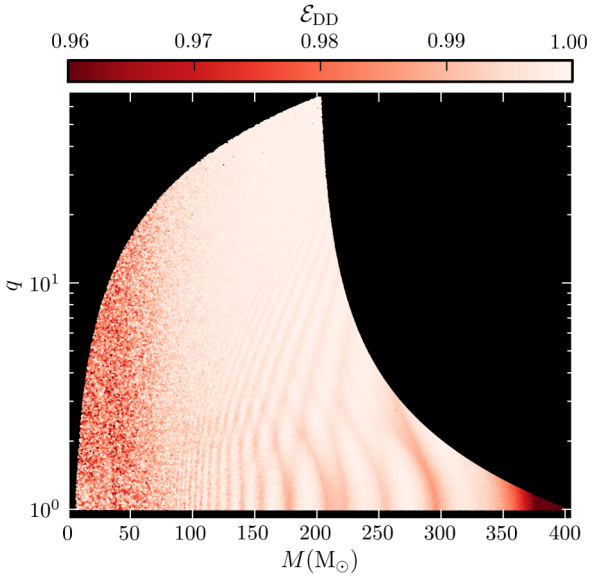

FIG. 1 (color online). Effectualness of a template bank placed using the 1.5 PN metric and using waveforms without subdominant modes (EOBNRv2) to injections without subdominant modes (also EOBNRv2), $\mathcal{E}_{\rm DD}$. The desired minimal match of the bank ($= \min\{\mathcal{E}\}$) is 0.97.

between a waveform with intrinsic parameters $\boldsymbol{\Upsilon}$ and a waveform with parameters $\boldsymbol{\Upsilon} + \delta\boldsymbol{\Upsilon}$ [11,12]. This metric is found analytically using inspiral waveforms expanded to 1.5 post-Newtonian order (PN) in phase [50].[12] As this metric is based solely on the inspiral part of the waveform, it will fail to properly place templates at high mass, where the waveforms are dominated by merger and ringdown [51]. More sophisticated template placement methods have recently been devised: a new metric has been calculated using the 3.5 PN approximant [52] and a "stochastic" placement method has been developed that uses no metric [53]. In this study we are only interested in the relative difference in sensitivity when a template bank neglects subdominant modes and not on the most efficient placement algorithm. We therefore use the same 1.5 PN placement algorithm that has been used in prior searches,[13] putting a cut on total mass where the metric fails to maintain the desired 97% minimal match.

To determine where the 1.5PN metric fails to maintain a 97% minimal match we generate a template bank to cover component masses between 3 and 200 $\mathrm{M}_\odot \times (6 \leq M/\mathrm{M}_\odot \leq 400)$. Using the aLIGO zero-detuned high power PSD, this results in a bank of 19800 templates. We calculate the effectualness of this bank to the injections without subdominant modes, $\mathcal{E}_{\rm DD}$; the results are shown in Fig. 1. The effectualness appears to be > 0.97 for $M \lesssim 360\ \mathrm{M}_\odot$, but is lower than that for larger M. Indeed, we find that less than 0.3% of injections with $M < 360\ \mathrm{M}_\odot$ have an effectualness < 0.97 [see Fig. 3], but ~70% of injections have an effectualness < 0.97 for total masses larger than 360 $\mathrm{M}_\odot$. We therefore place a cutoff of $M < 360\ \mathrm{M}_\odot$ when reporting effectualness and efficiency.

B. Efficiency to injections with subdominant modes

Figures 2 and 3 show the effectualness of the dominant-mode bank when subdominant modes are added to the injections, $\mathcal{E}_{\rm DS}$. We find that $\mathcal{E}_{\rm DS}$ is substantially lower than $\mathcal{E}_{\rm DD}$ for many injections: ~50% of subdominant injections have an effectualness < 0.97 for $M < 360\ \mathrm{M}_\odot$. In Fig. 2 we see that the effectualness decreases with increasing mass ratio. This is expected as the amount of power in the higher modes will increase relative to the dominant mode as the binary becomes more asymmetric.

Given that $\mathcal{E}_{\rm DS} < \mathcal{E}_{\rm DD}$ we wish to know if the predicted detection rates for advanced LIGO will be worse than expected. As discussed in Sec. II C we cannot tell this from effectualness alone. Instead, we compute $\mathcal{G}^{\rm DS}_{\rm DD}$, which is the sensitive volume of injections with subdominant modes ($V_{\rm DS}$) relative to the sensitive volume of injections without subdominant modes ($V_{\rm DD}$) when both are recovered by the dominant-mode template bank. If $\mathcal{G}^{\rm DS}_{\rm DD} < 1$ it means that the sensitivity to real signals (which have subdominant modes) will be worse than predicted. If $\mathcal{G}^{\rm DS}_{\rm DD} > 1$ it means that the

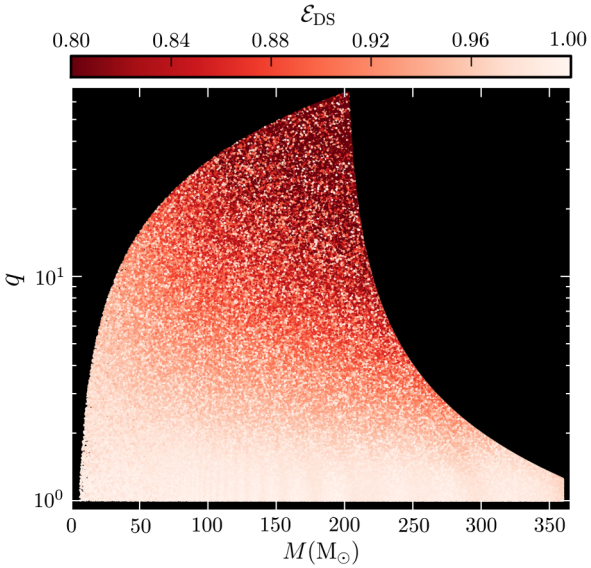

FIG. 2 (color online). Effectualness of the 1.5 PN dominant-mode template bank to injections with subdominant modes, $\mathcal{E}_{\rm DS}$. The desired minimal match ($= \min\{\mathcal{E}\}$) of the bank was 0.97, but we see that the effectualness drops below this as we go to higher mass ratio.

[12]In Ref. [50], the metric was calculated to *second* post-Newtonian order. However, a bug was recently discovered in the template-placement code in LAL (on which this study depends) that caused the metric calculation to be truncated at 1.5 PN. Since this bug was discovered after we had finished all calculations, we simply use the 1.5 PN metric.

[13]We emphasize that while the templates are *placed* using the 1.5 PN approximant, the template waveforms are EOBNRv2.

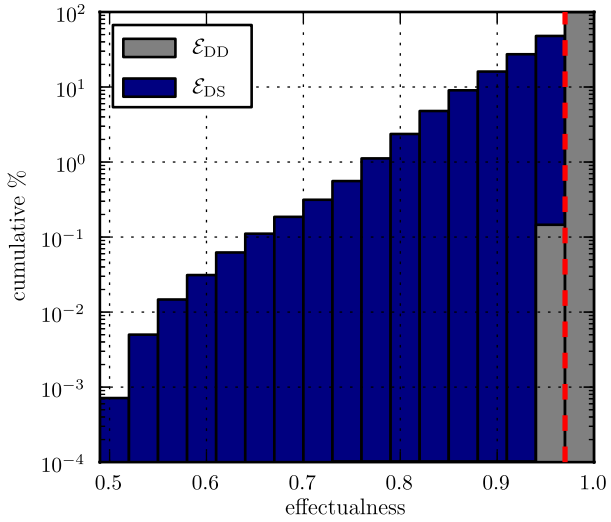

FIG. 3 (color online). Cumulative histogram of the effectualness of a template bank without subdominant modes to injections without subdominant modes $\mathcal{E}_{\rm DD}$ (gray) and injections with subdominant modes $\mathcal{E}_{\rm DS}$ (blue). Each bin gives the fraction of injections with an effectualness less than the right edge of the bin. The red dashed line indicates the target minimal match for the bank (0.97). All injections have total mass $< 360\ {\rm M}_\odot$.

sensitivity to real signals will be better than predicted; if $\mathcal{G}^{\rm DS}_{\rm DD} = 1$ it means there is no difference.

Figure 4 shows $\mathcal{G}^{\rm DS}_{\rm DD}$ in each mass bin. We see that the gain $\approx$1 everywhere. Indeed, if we assume a uniform astrophysical rate in component masses we find $\text{net}\{\mathcal{G}^{\rm DS}_{\rm DD}\} = 1.005 \pm 0.004$; a uniform rate in M and q yields $\text{net}\{\mathcal{G}^{\rm DS}_{\rm DD}\} = 1.019 \pm 0.004$. This means that a dominant-mode template bank yields predicted detection rates even though both the bank and the predictions neglect subdominant modes.

Comparing Fig. 4 to Fig. 2 we see that $\mathcal{G}^{\rm DS}_{\rm DD} \approx 1$ despite the drop in effectualness to injections with subdominant modes. Notably, the relative gain is slightly *larger than* 1 in the areas where the effectualness is *smallest*. This means that the drop in effectualness seen in Fig. 2 is largely due to an increase in the amount of power in injections when subdominant modes are added rather than a decrease in SNR between the templates and injections.

A decrease in effectualness will always result in an increase in χ^2, regardless of whether the mismatch ($\equiv 1 - \mathcal{E}$) results in an increase or decrease in SNR. Whether reweighted SNR increases or decreases therefore depends on whether the gain in ρ offsets the gain in χ^2. Figure 5 shows reduced χ^2 versus SNR for all injections with $M < 360\ {\rm M}_\odot$. The black arrows indicate how, on average, the injections move in this plane when higher modes are added. The solid black line shows where $\tilde{\rho} = 8$, which is the threshold we use when calculating efficiency. All injections to the left of this line are missed, all injections to the right are found. We see that at this threshold the increase in χ^2 is roughly offset by the increase in SNR when subdominant modes are added, which explains why $\mathcal{G}^{\rm DS}_{\rm DD} \approx 1$ despite an increase in mismatch for injections with subdominant modes.

Figure 5 also shows that as we go to higher ρ, the gain in χ^2_r becomes larger relative to the gain in SNR when subdominant modes are included (the black arrows progressively point to higher χ^2_r rather than to higher SNR as we move to the right in the plot). If our threshold $\tilde{\rho}$ were larger more injections would move below threshold (from an increase in χ^2) than above (from an increase in ρ). This is confirmed by Fig. 6. The top plot shows the percentage of injections that move above threshold (gained) and the percentage of injections that move below threshold (lost) when subdominant modes are added, as a function of threshold $\tilde{\rho}$. Around a threshold of $\tilde{\rho} = 8$ there is a small net

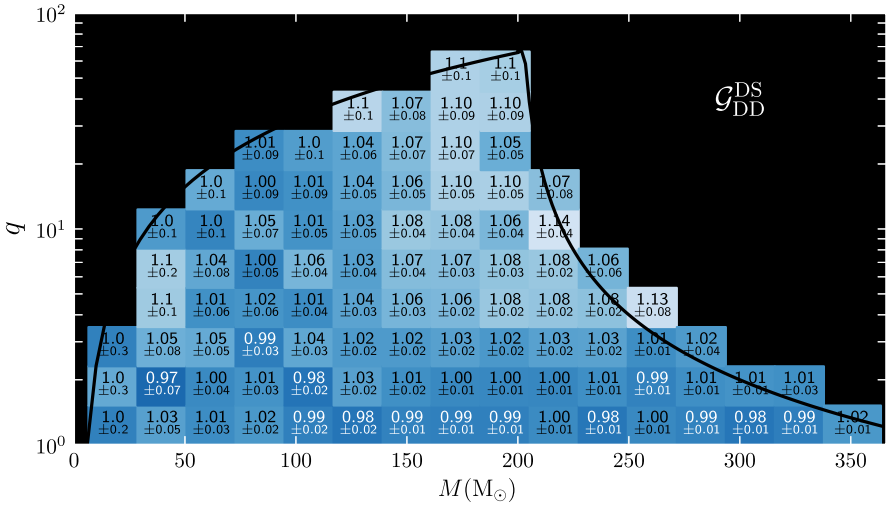

FIG. 4 (color online). Sensitive volume of injections with subdominant modes relative to sensitive volume of injections without subdominant modes when both are recovered by the dominant-mode template bank ($\mathcal{G}^{\rm DS}_{\rm DD}$; see Sec. II C for definition) in M, q plane. The solid black line indicates the injection region. Only tiles with 1000 or more injections in them are shown.

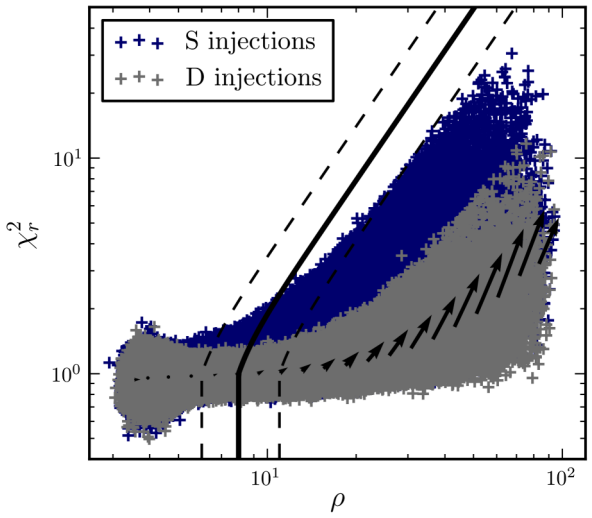

FIG. 5 (color online). Reduced χ^2 (χ^2_r) versus SNR of all injections with $M < 360\ \mathrm{M}_\odot$. Gray crosses are injections with the dominant-mode only; dark-blue crosses are injections with subdominant modes. The dashed and sold black lines show lines of constant $\tilde{\rho}$; shown are $\tilde{\rho} = 6$, 8, and 11 (dashed, solid, and dashed lines, respectively). The black arrows indicate where, on average, injections move in this plane when subdominant modes are added.

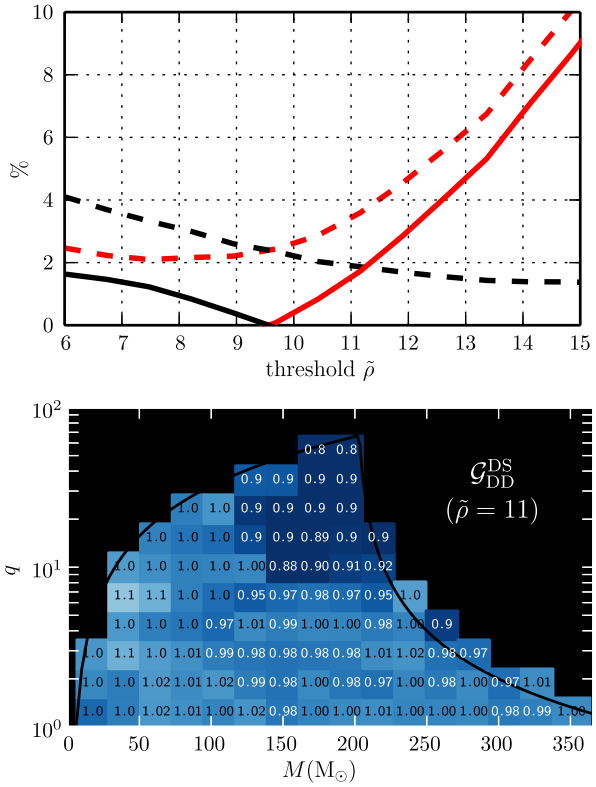

FIG. 6 (color online). Top: percentage of injections gained and lost when subdominant modes are added as a function of threshold $\tilde{\rho}$. The dashed black line shows the percentage of injections gained; the dashed red line shows the percentage of injections lost. The solid line shows the net gain/loss; where it is black there is a net gain; where it is red there is a net loss. Bottom: $\mathcal{G}^{\mathrm{DS}}_{\mathrm{DD}}$ when the threshold reweighted SNR for both D and S injections is 11 instead of 8. The solid black line indicates the injection region. Errors on gain are approximately twice the errors reported in the corresponding tiles in Fig. 4.

gain in the number of injections found when subdominant modes are added. If the threshold were larger than ~9.5, however, there would be a net loss. This loss causes an overall drop in efficiency, which in turn causes a drop in sensitivity. For example, the bottom plot in Fig. 6 shows $\mathcal{G}^{\mathrm{DS}}_{\mathrm{DD}}$ when the threshold $\tilde{\rho} = 11$. We see that many tiles have gains < 1 now. Assuming a uniform astrophysical rate in component-masses yields $\mathrm{net}\{\mathcal{G}^{\mathrm{DS}}_{\mathrm{DD}}\} = 0.994 \pm 0.004$; uniform in M, q yields $\mathrm{net}\{\mathcal{G}^{\mathrm{DS}}_{\mathrm{DD}}\} = 0.988 \pm 0.006$. Note, however, that the decrease in gain mostly occurs for tiles with $M > 100\ \mathrm{M}_\odot$ and $q > 4$, which is where the drop in effectualness is the largest. If we restrict our net gain calculation to stellar-mass BBHs only ($M < 100\ \mathrm{M}_\odot$) we get $\mathrm{net}\{\mathcal{G}^{\mathrm{DS}}_{\mathrm{DD}}\} = 1.01 \pm 0.03$ for both rate priors.

We conclude that if gravitational waves can be detected at a single detector $\tilde{\rho} \approx 9.5$ or less, then neglecting subdominant modes will not affect the expected sensitivity of a nonspinning BBH search across all masses. If the threshold for detection is larger, then neglecting subdominant modes will cause a larger drop in sensitivity than what would otherwise be expected for BBHs with $q \gtrsim 4$ and containing at least one IMBH ($m \gtrsim 100\ \mathrm{M}_\odot$). Nonspinning stellar-mass BBHs, however, are not affected by neglecting subdominant modes, even if the single-detector threshold for detection is $\tilde{\rho} = 11$.

IV. PREDICTED EFFICIENCY OF A TEMPLATE BANK WITH SUBDOMINANT MODES

In the previous section we found that neglecting subdominant modes did not adversely affect the sensitivity of a search for nonspinning BBHs. We found this by comparing the sensitive volume of injections with subdominant modes to the sensitive volume of injections without subdominant modes when both are recovered by dominant-mode templates. However, the decrease in effectualness to injections with subdominant modes means that there is some power not being recovered by the dominant-mode templates. If the templates had subdominant modes they would be able to recover that power, which could increase the sensitivity of the search. We therefore wish to know how the sensitivity of a bank of templates with subdominant modes compares to a bank of templates without subdominant modes, $\mathcal{G}^{\mathrm{SS}}_{\mathrm{DS}}$.

A. Search sensitivity when subdominant modes are included in all templates

Currently, no search exists that uses a bank of templates with subdominant modes. We do not try to create one here. Instead, we simulate how such a search would perform as compared to the dominant-mode template bank used here.

In our simulation we will continue to use $\tilde{\rho}$ maximized over the template bank as our detection statistic. We do not try to find the optimal search statistic when subdominant modes are used. As discussed in Sec. II C 1, finding the optimal statistic over a bank of templates is difficult, if not impossible, due to our lack of knowledge of the mass distribution of BBHs. Our goal here is to answer the question: using current search techniques, will sensitivity improve if we include subdominant modes in templates?

To calculate $\mathcal{G}^{\mathrm{SS}}_{\mathrm{DS}}$ we need to know the sensitive volume of a template bank with subdominant modes to injections with subdominant modes, V_{SS}. Since V_{SS} depends on the number of injections found by the template bank above some threshold, finding V_{SS} requires two pieces of information: the average reweighted SNR of injections filtered with a subdominant mode template bank $\langle\tilde{\rho}_{\mathrm{SS}}\rangle$, and the threshold for making a detection in such a search.

In order to estimate $\langle\tilde{\rho}_{\mathrm{SS}}\rangle$ of each injection we first calculate the maximum SNR that can be recovered from the injection by finding the overlap of the injection with itself [see Eq. (14)]. A real subdominant mode search will use discrete templates, as is done with the dominant-mode bank. The discreteness of the template bank will cause some loss of SNR. Even though both the injections and templates have subdominant modes in our simulation, the mismatch due to the discreteness of the bank will also cause some small increase in χ^2_r, as was the case for the dominant-mode injections recovered by the dominant-mode template bank (gray crosses in Fig. 5). This in turn causes a small decrease in reweighted SNR relative to SNR for some injections. To simulate both of these effects, we estimate $\langle\tilde{\rho}_{\mathrm{SS}}\rangle$ to be

$$\langle\tilde{\rho}_{\mathrm{SS}}\rangle = \frac{\langle\tilde{\rho}_{\mathrm{DD}}\rangle}{\langle\rho_{\mathrm{DD}}\rangle}\mathcal{E}_{\mathrm{DD}}\max\{\rho_{\mathrm{SS}}\}. \tag{22}$$

Here $\mathcal{E}_{\mathrm{DD}}$ simulates the loss in SNR due to the discreteness of the bank—i.e., we have assumed $\langle\rho_{\mathrm{SS}}\rangle \approx \mathcal{E}_{\mathrm{DD}}\max\{\rho_{\mathrm{SS}}\}$—and $\langle\tilde{\rho}_{\mathrm{DD}}\rangle/\langle\rho_{\mathrm{DD}}\rangle$ simulates the effect of χ^2_r reweighting. Thus the discreteness of our simulated template bank with subdominant modes is equivalent to the discreteness of our (real) dominant-mode bank.

By assuming $\langle\rho_{\mathrm{SS}}\rangle \approx \mathcal{E}_{\mathrm{DD}}\max\{\rho_{\mathrm{SS}}\} = \mathcal{E}_{\mathrm{DD}}\sqrt{\langle h_{\mathrm{S}}, h_{\mathrm{S}}\rangle}$ in Eq. (22) we have neglected any contribution to the SNR from noise. Due to the maximization over the phase, the average SNR of a simulated signal h when filtered with itself in Gaussian noise will be slightly larger than $\sqrt{\langle h, h\rangle}$. Rather than adding a factor to our estimate of $\langle\tilde{\rho}_{\mathrm{SS}}\rangle$ to account for this contribution, when finding $\mathcal{G}^{\mathrm{SS}}_{\mathrm{DS}}$ we use a "noiseless" estimate of $\langle\tilde{\rho}_{\mathrm{DS}}\rangle$, given by

$$\langle\tilde{\rho}_{\mathrm{DS}}\rangle^{(\mathrm{noiseless})} = \frac{\langle\tilde{\rho}_{\mathrm{DS}}\rangle}{\langle\rho_{\mathrm{DS}}\rangle}\mathcal{E}_{\mathrm{DS}}\max\{\rho_{\mathrm{SS}}\}. \tag{23}$$

Here, $\mathcal{E}_{\mathrm{DS}}\max\{\rho_{\mathrm{SS}}\}$ gives $\langle\rho_{\mathrm{DS}}\rangle$ with the noise contribution removed and $\langle\tilde{\rho}_{\mathrm{DS}}\rangle/\langle\rho_{\mathrm{DS}}\rangle$ accounts for χ^2_r reweighting.

When calculating the sensitivity of the dominant-mode template bank we used a threshold of $\tilde{\rho} = 8$. In a real search triggers are produced by gravitational waves and by background noise. High statistical significance is therefore required in order for a trigger to be considered a gravitational-wave candidate. The standard measurement of significance is false-alarm probability $\mathcal{F}(\rho)$. When evaluating the sensitivity of the dominant-mode template bank we choose $\tilde{\rho} = 8$ because it corresponds to a false-alarm probability small enough that we could confidently claim detection in real detector data. This means that to compare the sensitivity of the simulated subdominant mode search to the dominant-mode search we must chose a threshold $\tilde{\rho}$ that results in the same false-alarm probability that $\tilde{\rho} = 8$ did in the dominant-mode search.

As discussed in Sec. II A subdominant modes break the degeneracy between θ, ϕ and κ. This means that to fully recover all of the power in the subdominant modes we have to maximize over three extrinsic parameters instead of one. These additional maximizations will cause the single-detector SNR distribution in noise to change. SNR from dominant-mode templates is χ distributed with 2 degrees of freedom in stationary Gaussian noise. If a template has subdominant modes, the SNR will have a larger number of degrees of freedom. The increase in the degrees of freedom means that $\mathcal{F}(\rho)$ at a given SNR will increase. In order to keep the same false-alarm probability for a bank with subdominant modes as we had for the dominant-mode bank, the threshold $\tilde{\rho}$ must therefore increase. The relative gain in sensitivity of a template bank with subdominant modes depends on whether the increase in SNR due to the subdominant modes is enough to offset the increase in SNR threshold.

In Appendix B we estimate the false-alarm probability of a dominant-mode template bank with N templates $\mathcal{F}(\rho|\mathrm{D}, N)$ at $\rho = 8$ [see Eq. (B2)]. For the dominant-mode bank used here $N = 19800$, which gives $\mathcal{F}(\rho = 8|\mathrm{D}, N) \approx 2.5 \times 10^{-10}$. We also calculate false-alarm probability as a function of SNR of the simulated subdominant mode bank $\mathcal{F}(\rho|\mathrm{S}, N)$ [see Eqs. (B1) and (B6)]. Assuming $\tilde{\rho} \approx \rho$ for injections, we estimate that the threshold $\tilde{\rho}$ would have to increase to 8.31 for the subdominant mode bank in order for $\mathcal{F}(\rho|\mathrm{S}, N)$ to also be equal to 2.5×10^{-10}.

Using the estimated $\tilde{\rho}_{\mathrm{SS}}$ given in Eq. (22) and a threshold $\tilde{\rho} = 8.31$ we calculate the sensitive volume of the simulated subdominant mode template bank V_{SS} in the same M, q tiles we used in Fig. 4. We compare this to V_{DS} (which used a threshold $\tilde{\rho} = 8$) to get $\mathcal{G}^{\mathrm{SS}}_{\mathrm{DS}}$; this is plotted in Fig. 7. We find that the subdominant mode template bank has *worse* sensitivity then the dominant-mode bank across nearly the entire mass space, dropping to as low as ~90% for mass ratios between 1 and 1.5.

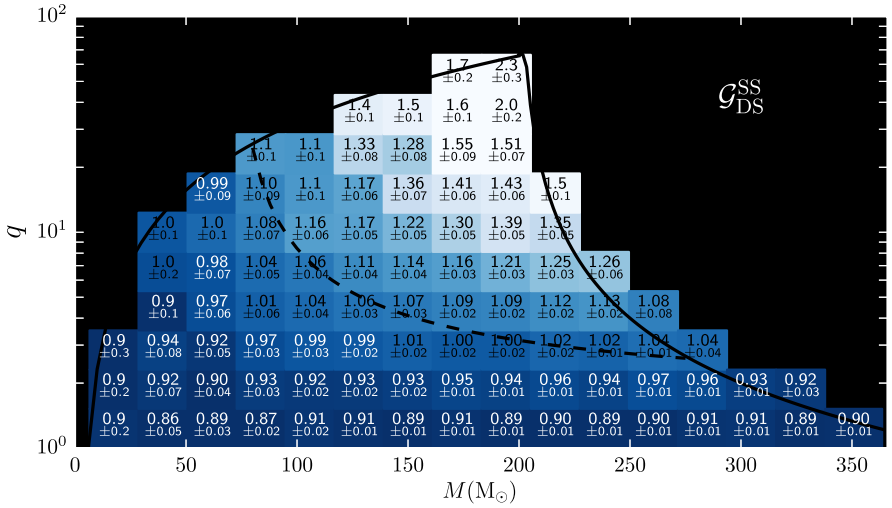

FIG. 7 (color online). Relative gain of subdominant bank compared to dominant-mode bank if the subdominant modes are used everywhere, $\mathcal{G}^{\rm SS}_{\rm DS}$. The solid black line indicates the injection region. The dashed black line shows where we choose to place a boundary between dominant-mode and subdominant mode templates for a split-bank search (see Fig. 9 for gain).

The reason for the poor sensitivity of the subdominant mode bank to equal-mass systems can be understood by considering Fig. 2, in which we see that when $q \to 1$, $\mathcal{E}_{\rm DS} \to 1$. This means that dominant-mode templates are recovering nearly all of the available power in equal-mass signals. Put another way, signals from equal-mass systems gain almost no SNR by adding subdominant modes to the templates. The SNR distribution in noise of subdominant mode templates that are close to the equal-mass line are not much different than their dominant-mode counterparts. However, false-alarm probability is a *global* property of the template bank: even though the SNR distribution does not change for equal-mass templates, it does for more asymmetric-mass templates. The presence of these templates in the bank affects the false-alarm probability of the entire search. The result is that equal-mass signals suffer an increase in threshold but gain no SNR from the subdominant template bank.

The subdominant mode bank does have better sensitivity at higher mass ratios and total masses. In the highest mass-ratio tile in Fig. 2 the sensitivity is twice that of a dominant-mode bank. A subdominant mode bank may therefore still increase the probability of making a detection, if the total gain in sensitive volume to higher mass-ratio systems is enough to offset the drop in sensitivity to equal-mass systems. However, assuming either a uniform astrophysical rate in m_1, m_2 or a uniform rate in M, q, yield net gains < 1: the former gives $\mathrm{net}\{\mathcal{G}^{\rm SS}_{\rm DS}\} = 0.932 \pm 0.003$ while the latter gives $\mathrm{net}\{\mathcal{G}^{\rm SS}_{\rm DS}\} = 0.987 \pm 0.003$. Restricting to stellar-mass BBHs also results in net gains < 1, yielding 0.92 ± 0.01 and 0.96 ± 0.01 for the two priors, respectively.

Using templates that more accurately model signals should improve sensitivity. The reason the subdominant mode templates do not is due to the astrophysical prior that is inherent in the search. Simply selecting the template with the largest SNR when maximizing over the bank (as we have done for both the dominant-mode and subdominant mode bank, and as is done in current searches) assumes that every template is equally likely to detect a signal. The detectors are not equally sensitive to all signals, however, nor is the density of templates uniform. This makes the search most sensitive to a particular astrophysical rate distribution. Adding subdominant modes changes the distribution to which the search is most sensitive, thereby implicitly changing the search prior.

As noted by Refs. [14] and [15], the largest SNR increase occurs for signals from asymmetric-mass binaries and from systems inclined to the line of sight. Yet the magnitude of the detector's sensitivity is lowest to these systems. Including subdominant modes while weighting the SNR of each template equally causes us to gain sensitivity to signals for which we are least sensitive at the cost of losing sensitivity to signals for which we are most sensitive. We can see this negative correlation in Fig. 8, which shows the fractional gain in SNR when subdominant modes are added (ignoring the effects of χ^2_r reweighting) versus the distance at which a signal can be detected by the dominant-mode bank at SNR 8 ("sensitive distance"), colored by mass ratio. The sensitive distance of the signals with the largest gain (and mass ratio) is an order of magnitude smaller than the sensitive distance of the signals with the smallest gain. In general, a plot such as this can be used to determine whether or not changing the parameters of a search are worthwhile. If there is a negative correlation between SNR gain and sensitive distance—i.e., only signals for which the detector is least sensitive gain SNR by changing the search parameters—that change is unlikely to improve the overall detection rate unless the astrophysical distribution is strongly weighted to those signals.

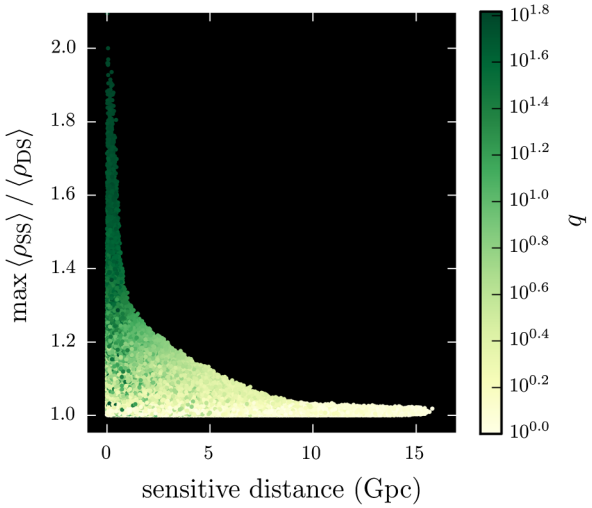

FIG. 8 (color online). The maximum gain in SNR that is possible by adding subdominant modes to templates ($\max\langle\rho_{SS}\rangle/\langle\rho_{DS}\rangle$) versus the distance at which a signal can be detected by the dominant-mode template bank at SNR 8 (sensitive distance). Each point represents a simulated signal; the points are colored by their mass-ratio (q).

B. Splitting the template bank to improve sensitivity

Including subdominant modes in templates would improve the sensitivity of the search if we applied a weight to each template that better reflected the probability the template will make a detection. Determining the best weight to use requires knowledge of the astrophysical rate of signals. We expect that signals will be distributed uniformly in the inclination angle θ. However, the proper weight to apply to signals with this assumption is already inherent in the SNR. The projection of the waveform into the radiation frame, and then again into the detector's frame (done by the **P** and **K** matrices, respectively, in Appendix A) *is* the weight one should apply to the SNR assuming signals are distributed uniformly in space. Indeed, that the SNR from an inclined signal is smaller than the SNR from a face-on signal at the same distance is a result of the antenna pattern indicating that these signals are less likely to be detected.

Any weight we apply to the SNR must therefore be based on the distribution of intrinsic paramters. Given the large uncertainty in the mass distribution of BBHs this is difficult to do. However, if we can find a weight that results in $\mathcal{G} \geq 1$ relative to the dominant-mode search in all mass tiles, we know that this new search will be at least as sensitive to real signals as the dominant-mode search, regardless of the astrophysical mass distribution.

The simplest way to arrive at such a weight is to split the template bank in two parts. In one part we use templates with subdominant modes; in the other, we use dominant-mode templates. In this scenario false-alarm probabilities are calculated separately in each region, then combined. As we will see below, the process of combining the results across the split effectively down-weights higher mass-ratio templates such that they do not hurt the sensitivity to equal-mass systems, yet they still improve sensitivity to the high-mass ratio signals.

In order to not lose any sensitivity we need to place the split between dominant-mode and subdominant mode templates at points in the mass space where $\mathcal{G}^{SS}_{DS} > 1$. Otherwise, signals with masses that are in the subdominant part of the bank that are near the split will suffer a loss of sensitivity. We empirically chose to split the bank such that subdominant mode templates are used when[14]

$$m_2 < 0.6\, m_1 - 43. \tag{24}$$

This cut is shown in Fig. 7 (black dashed line). We note that this is an empirical estimate for this template bank and Gaussian noise. If a real search were performed, this cut would have to be tuned based on the noise and bank characteristics. We assume that such a cut would be in approximately the same location in parameter space as the cut we choose here, however.

Using the split in Eq. (24) we find that 3750 templates are in the subdominant region while 16050 templates remain in the dominant-mode region. In Appendix B we find that $\mathcal{F}(\rho)$ is roughly proportional to the number of templates in the search [see Eq. (B1)]. This means that the false-alarm probabilities we get for triggers in the dominant-mode part of the template bank will have decreased by a factor of $16050/19800 \approx 0.8$ compared to what we get when we search the entire mass space. Likewise, the false-alarm probability of triggers in the subdominant mode part of the bank will decrease by a factor of ~0.2. These drops in false-alarm probabilities are artificial: they are due solely to our choice of cut. Indeed, we could split the bank an arbitrary number of times, thereby arbitrarily decreasing false-alarm probabilities.

To account for this artificial decrease we must combine results by multiplying the signals' false alarm probabilities by a *trials factor* [6]. For the dominant-mode part of the bank we multiply by $19800/16050 \approx 1.2$; this is equivalent to using dominant mode templates throughout the entire mass space, and so the threshold in this part of the bank remains $\tilde{\rho} = 8$. In the subdominant mode part of the bank we multiply by $19800/3750 \approx 5.3$. To keep $\mathcal{F}(\rho)$ fixed at 2.5×10^{-10}, the threshold in this region increases to 8.44. This is equivalent to down-weighting $\tilde{\rho}$ of templates in this part of the bank, as desired.

Figure 9 shows the relative gain of the split bank (indicated by $\frac{S}{D}$) compared to using dominant mode templates everywhere ($\mathcal{G}^{\frac{S}{D}S}_{DS}$). We find that we can gain sensitivity by using templates with subdominant modes if

[14]We put the cut in m_1, m_2 rather then M, q because we found that the $\mathcal{G}^{SS}_{DS}$ was roughly linear in m_1, m_2.

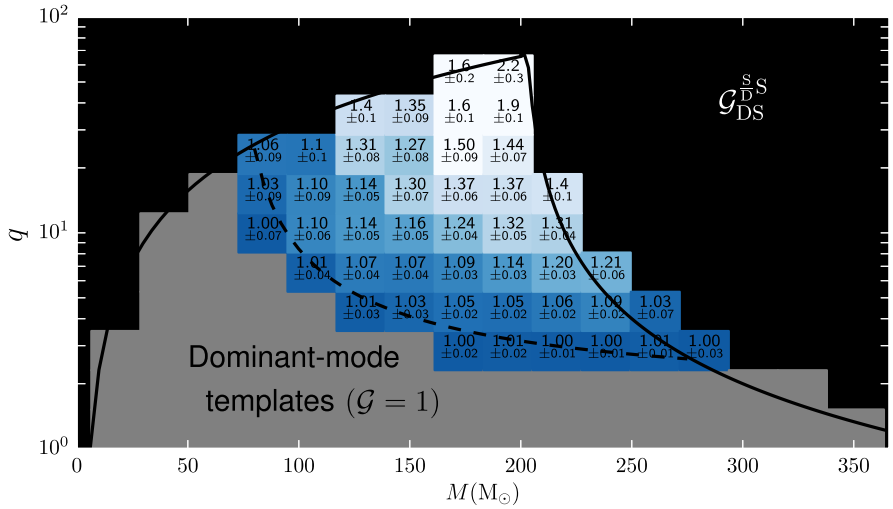

FIG. 9 (color online). Relative gain of subdominant bank compared to dominant-mode bank if the subdominant modes are only used in part of the bank, $\mathcal{G}^{\mathrm{S}\,\mathrm{S}}_{\mathrm{D}\,\mathrm{S}}$. The sold black line indicates the injection region; the dashed-black line indicates the boundary used for switching between dominant-mode and subdominant mode templates.

we split the bank using the criteria in Eq. (24). Since dominant-mode templates are used below this cut, we lose no sensitivity relative to what we had when we used dominant-mode templates everywhere. In terms of possible astrophysical systems, note that only IMRIs ($m_1 \gtrsim 100\ \mathrm{M}_\odot$, $m_2 \lesssim 80\ \mathrm{M}_\odot$) fall in the region where subdominant modes are used, and that the dominant-mode part of the bank covers all possible stellar-mass BBHs (m_1, $m_2 \lesssim 80\ \mathrm{M}_\odot$).

Splitting the bank and only using subdominant modes in one part results in a search that is as good or better than the dominant-mode search in all mass tiles, as we desired. The net gain, however, is not much larger than simply using dominant-mode templates everywhere. Assuming a uniform astrophysical rate in component masses gives $\mathrm{net}\{\mathcal{G}^{\mathrm{S}\,\mathrm{S}}_{\mathrm{D}\,\mathrm{S}}\} = 1.002 \pm 0.004$; assuming a uniform rate in M, q yields 1.024 ± 0.004. The reason for the nearly nonexistent increase in net gains can be understood by considering Fig. 10, which shows the sensitive volume of the split bank in Gpc^3. For a given total mass, the largest sensitivity occurs at equal mass by a large margin. For example, between ~190 and 200 $\mathrm{M}_\odot$ (the mass bin with the largest range in q) we see that the sensitive volume drops by 4 orders of magnitude—from 526 Gpc^3 to 0.43 Gpc^3—as we go from $q = 1$ to $q \approx 60$. Even though the subdominant modes have doubled our sensitivity at the highest mass ratio tile, the magnitude of the sensitive volume is small relative to the other parts of the bank. Using the split bank is therefore unlikely to have a significant effect on the overall probability of making a gravitational-wave detection in advanced LIGO, unless there is a relatively large population of IMRIs with $q \gtrsim 4$ compared to IMBH-IMBH and stellar-mass BBHs.

V. CONCLUSIONS AND FUTURE WORK

We have investigated the effects of neglecting subdominant modes in templates on the predicted BBH sensitivity of a single advanced LIGO detector. In doing so we have considered the loss in reweighted SNR, which more accurately reflects what is done in real BBH searches than considering SNR alone. We found that not including subdominant modes in templates does not make the sensitivity to nonspinning BBH signals any worse than what has been predicted as long as the gravitational waves can be detected at single-detector reweighted SNRs $\lesssim$9.5. If the threshold for detection is larger, neglecting subdominant modes will result in worse sensitivity than predicted, but only for IMRI BBHs with total masses $\gtrsim$100 $\mathrm{M}_\odot$ and $q \gtrsim 4$. Stellar-mass BBHs ($M \lesssim 100\ \mathrm{M}_\odot$) and more equal-mass IMBH-IMBH binaries ($m_{1,2} \gtrsim 100\ \mathrm{M}_\odot$, $q \lesssim 4$) are unaffected.

We have also simulated a bank of nonspinning templates that have subdominant modes to see if any improvement in sensitivity can be gained. To do so we analytically maximized the SNR over κ when subdominant modes are included, then numerically maximized over the remaining extrinsic parameters [see Appendix A]. We found that if subdominant modes are used throughout the entire bank, and all templates are weighted equally, the sensitivity would be *worse* for stellar-mass BBHs and IMBH-IMBH binaries with $q \lesssim 4$ due to the increase in threshold needed to keep false-alarm probability fixed. Such a search would only improve sensitivity to IMRIs with $q \gtrsim 4$. Therefore, in order to include subdominant modes in templates, the templates must be weighted by the likelihood that they will detect a signal.

We found an effective weight by splitting the bank in two parts. Using subdominant modes in templates that satisfy

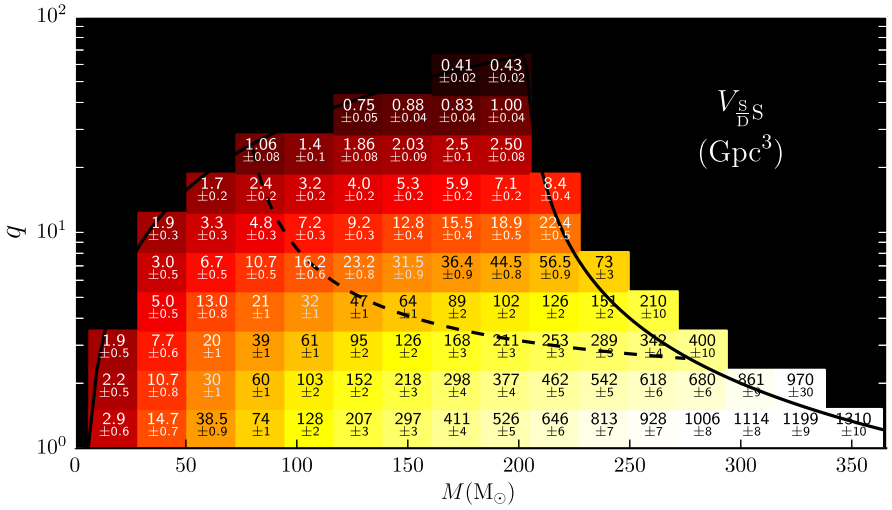

FIG. 10 (color online). Sensitive volume in Gpc^3 of the split bank. The solid-black line shows the injection region, the dashed-black line the cut between subdominant and dominant-mode templates. Dividing the sensitive volumes in this figure by the net gains given in Fig. 9 yields sensitive volumes if dominant-mode templates are used everywhere.

Eq. (24) and dominant-mode templates elsewhere, we can improve the sensitivity to IMRI BBHs without sacrificing the sensitivity to stellar-mass BBHs and IMBH-IMBH binaries. The split bank is only one of many possible weighting schemes. Using subdominant modes throughout the entire bank with a more incremental weight may yield better sensitivity. However, since subdominant modes improve sensitivity to signals for which the detectors are least sensitive, a more sophisticated search would probably only yield a small increase in the detection rate.

In Fig. 10 we present the single-detector sensitive volumes of the split bank. We find that the sensitive volumes to signals in the subdominant part of the bank (tiles above the black dashed line) are 1–4 orders of magnitude smaller than equal mass-ratio systems with equivalent total masses. Using the split bank is therefore unlikely to substantially increase the probability of making a gravitational-wave detection over a dominant-mode bank unless there is a large population of high-mass ratio IMRIs in the universe.

In order to use a split bank more investigation is required to establish how exactly to use subdominant modes in a real search. Open questions include how to search over θ and ϕ,[15] and how to apply a coincidence test between multiple detectors. Given that using a split bank has negligible impact on the overall probability of making a gravitational-wave detection in advanced LIGO, simply using a dominant-mode bank everywhere may be more desirable.

We did not try to predict advanced LIGO BBH detection rates, as doing so would require a choice of astrophysical rates. However, Fig. 10 can be used to predict detection rates if a particular astrophysical rate is assumed. The volumes given in Fig. 10 are for a split bank; dividing the sensitive volumes by the net gains given in Fig. 9 yields the sensitive volumes if a dominant-mode bank is used everywhere instead. For example, if a dominant-mode bank is used, the sensitive volume of the largest-mass ratio tile is $\sim$0.2 Gpc^3 instead of 0.43 Gpc^3. The sensitive volumes we report were calculated using a single detector. Since real searches use a network of detectors, actual sensitive volumes may vary depending on the relative sensitivities of each detector.

We emphasize that in this study we only considered nonspinning signals. Subdominant modes are likely to play a more important role when one or both of the component masses are spinning. Currently, there are no spinning waveform models available with merger and ringdown that include subdominant modes. Once such waveforms become available, creating a subdominant mode search may be more advantageous. Since our analytic maximization over κ in Appendix A is still valid if the component masses are spinning, the result therein [specifically Eq. (A20)] can be used in such a search.

A dominant-mode EOB model calibrated to numerical relativity that incorporates spins aligned with the orbital angular momentum does currently exist [54], as well as spinning "phenomological" models derived from numerical relativity [55,56]. Past BBH searches have only used nonspinning templates, but there is much work currently ongoing to extend template banks into the spinning regime [53,57]. Doing so brings up many of the same questions we addressed in this study: Is the sensitivity of a search significantly affected by neglecting spin? Does the increase in number of templates needed to include spin increase the false-alarm probability such that any gain in SNR is nullified? In a future work we will

[15]One possibility is to simply place templates in θ and ϕ using the stochastic method described in Ref. [53]. In that case, the SNR of each template would be found using Eq. (A20).

address these questions using spinning EOB waveforms calibrated to numerical relativity and the methods that we establish in this study.

ACKNOWLEDGMENTS

We are grateful to Kipp Cannon, Thomas Dent, Prayush Kumar, Cole Miller, Alex Nitz, and John Whelan for valuable discussions. We would also like to thank Duncan Brown for providing some of the software used in this analysis. A. B., C. C., and Y. P. acknowledge partial support from NSF Grants No. PHY-0903631 and No. PHY-1208881. A. B. also acknowledges partial support from the NASA Grant No. NNX12AN10G. All calculations were performed on the SUGAR cluster, which is supported by NSF Grants No. PHY-1040231, No. PHY-1104371, and No. PHY-0600953, and by Syracuse University ITS.

APPENDIX A: SNR MAXIMIZATION WITH SUBDOMINANT MODES

All of the assumptions we made for dominant-mode templates apply to templates with subdominant modes up to Eq. (8). As stated in Sec. II, when only the dominant mode is considered, the angles κ, θ, and ϕ can be combined into a single parameter. The maximization over this parameter is straightforward as the denominator of the SNR does not depend on it (the parameter cancels in the inner product $\sqrt{\langle h, h\rangle}$) [10]. However, when subdominant modes are considered, the maximization over the extrinsic parameters is more complicated. First, κ, θ, and ϕ cannot be combined as the degeneracy between them is broken. Second, both the numerator and the denominator in the SNR depend on all three angles [see Eq. (A19), below]. Here we derive an analytic expression for the SNR maximized over κ when all modes are included in the waveform. As the result [Eq. (A20)] has nontrivial dependence on θ and ϕ, we calculate the remaining maximizations numerically.

The m summation in Eq. (2) is over $-l \le m \le l$. The number of terms in the summation can be reduced by relating the positive and negative m modes. Letting

$$
\begin{aligned}
{}_{-2}Y_{lm}(\theta,\phi) &= g_{lm}(\theta)e^{im\phi},\\
h_{lm}(t) &= A_{lm}(t)e^{-im\Psi_{lm}(t)},
\end{aligned}
$$

h is

$$
\begin{aligned}
h(t) = \sum_{l|m|}(&\Re\{g_{lm}(\theta)e^{im\phi}h_{lm}(t)\\
&+ g_{l-m}(\theta)e^{-im\phi}h_{l-m}(t)\})\cos\kappa\\
&+ (\Im\{g_{lm}(\theta)e^{im\phi}h_{lm}(t)\\
&+ g_{l-m}(\theta)e^{-im\phi}h_{l-m}(t)\})\sin\kappa. \qquad \text{(A1)}
\end{aligned}
$$

Here, $|m|$ indicates that the summation is over positive-m modes only, and we have set $\mathcal{D} = 1$ since it does not enter in the SNR.[16] The $\pm m$ modes of the h_{lm} are related by

$$h_{l-m} = (-1)^l h^*_{lm}. \qquad \text{(A2)}$$

Using this relationship Eq. (A1) becomes

$$
\begin{aligned}
h(t) = \sum_{l|m|}&(G_{1lm}(\theta)\cos(m\phi)h_{1lm}(t)\\
&+ G_{1lm}(\theta)\sin(m\phi)h_{2lm}(t))\cos\kappa\\
&+ (G_{2lm}(\theta)\sin(m\phi)h_{1lm}(t)\\
&- G_{2lm}\cos(m\phi)h_{2lm}(t))\sin\kappa, \qquad \text{(A3)}
\end{aligned}
$$

where

$$G_{1lm}(\theta) = g_{lm}(\theta) + (-1)^l g_{l-m}(\theta); \qquad \text{(A4)}$$

$$G_{2lm}(\theta) = g_{lm}(\theta) - (-1)^l g_{l-m}(\theta); \qquad \text{(A5)}$$

$$h_{1lm}(t) = A_{lm}(t)\cos[m\Psi(t)]; \qquad \text{(A6)}$$

$$h_{2lm}(t) = A_{lm}(t)\sin[m\Psi(t)]. \qquad \text{(A7)}$$

Equation (A3) can be expressed more concisely by the matrix equation

$$h(t) = \sum_{l|m|}\mathbf{K}\mathcal{P}_{lm}\mathcal{H}_{lm} \qquad \text{(A8)}$$

$$= \mathbf{KPH}, \qquad \text{(A9)}$$

where

$$\mathcal{P}_{lm} = \begin{pmatrix} G_{1lm}\cos m\phi & G_{1lm}\sin m\phi \\ G_{2lm}\sin m\phi & -G_{2lm}\cos m\phi \end{pmatrix}; \qquad \text{(A10)}$$

$$\mathcal{H}_{lm} = \begin{pmatrix} h_{1lm} \\ h_{2lm} \end{pmatrix}; \qquad \text{(A11)}$$

$$\mathbf{K} = [\cos\kappa \quad \sin\kappa]; \qquad \text{(A12)}$$

$$\mathbf{P} = [\mathcal{P}_{22} \quad \mathcal{P}_{21} \quad \cdots]; \qquad \text{(A13)}$$

$$\mathbf{H} = \begin{bmatrix} \mathcal{H}_{22} \\ \mathcal{H}_{21} \\ \vdots \end{bmatrix}. \qquad \text{(A14)}$$

[16] As written, Eq. (A1) double counts terms for which $m = 0$. For the sake of brevity we have redefined the A_{l0} in this equation to be $1/2$ of their original values.

Let us define the *covariance matrix* $\mathbf{C}$ as

$$\mathbf{C} \equiv \mathbf{H} \otimes \mathbf{H}, \tag{A15}$$

where the outer product $\mathbf{A} \otimes \mathbf{B}$ is

$$[\mathbf{A} \otimes \mathbf{B}]_{ij} \equiv \langle A_i, B_j \rangle. \tag{A16}$$

Note that $\mathbf{K}$ depends only on κ, $\mathbf{P}$ on θ and ϕ, and $\mathbf{C}$ on the intrinsic parameters $\boldsymbol{\Upsilon}$. Also note that $\mathbf{C}$ is symmetric. In this notation $\langle h, h \rangle$ is

$$\langle h, h \rangle = \mathbf{KPCP^T K^T}. \tag{A17}$$

Defining $\mathbf{Q}$ as

$$\mathbf{Q} = \mathbf{H} \otimes [\, s \,] = \begin{bmatrix} \langle h_{122}, s \rangle \\ \langle h_{222}, s \rangle \\ \vdots \end{bmatrix} \tag{A18}$$

the SNR is

$$\rho = \max_{\theta,\phi,\kappa} \frac{\mathbf{KPQ}}{\sqrt{\mathbf{KPCP^T K^T}}}. \tag{A19}$$

We can perform the maximization over κ analytically. First consider the case when $\theta = \pi/2$. From the definition of the ${}_{-2}Y_{lm}$,

$$G_{2lm}(\pi/2) = 0, \qquad \forall (l, m),$$

which means

$$P_{2i}(\theta = \pi/2, \phi) = 0, \qquad \forall i.$$

In this case $\mathbf{KP}$ has no $\sin\kappa$ terms, causing the κ dependence to cancel in Eq. (A19). Thus[17]

$$\rho = \max_{\phi,\theta=\pi/2} \frac{P_{1i} Q_i}{\sqrt{P_{1j} C_{jk} P_{k1}}}.$$

To maximize over κ when $\theta \neq \pi/2$, let $\mathbf{g} = \mathbf{PCP^T}$ so that the denominator of the SNR is $\sqrt{\mathbf{KgK^T}}$. Note that $\mathbf{g}$ is a 2×2 symmetric matrix. We can therefore think of it as a metric that defines an inner product space between 2-dimensional vectors. Since $\mathbf{g}$ depends on $\mathbf{P}$ and $\mathbf{C}$ the curvature of this space is determined by θ, ϕ, and $\boldsymbol{\Upsilon}$. From this point of view the denominator of the SNR is simply the magnitude of $\mathbf{K}$ in this space:[18]

$$\sqrt{\mathbf{KPCP^T K^T}} = \sqrt{\mathbf{KgK^T}} \equiv \sqrt{\langle\langle \mathbf{K}, \mathbf{K} \rangle\rangle} \equiv ||\mathbf{K}||.$$

If we let $\mathbf{S^T} = \mathbf{g}^{-1}\mathbf{PQ}$ then we find that the numerator of the SNR is the inner product of $\mathbf{K}$ and $\mathbf{S}$:

$$\mathbf{KPQ} = \mathbf{KgS^T} = \langle\langle \mathbf{S}, \mathbf{K} \rangle\rangle.$$

The SNR is therefore at a maximum when $\mathbf{K}$ and $\mathbf{S}$ are aligned:

$$\rho = \max_{\theta,\phi,\kappa} \frac{\langle\langle \mathbf{S}, \mathbf{K} \rangle\rangle}{||\mathbf{K}||} = \max_{\theta,\phi} ||\mathbf{S}||.$$

The magnitude of $\mathbf{S}$ is

$$||\mathbf{S}|| = \sqrt{\mathbf{SgS^T}} = \sqrt{\mathbf{Q^T P^T} (\mathbf{g}^{-1})^{\mathbf{T}} \mathbf{g} \mathbf{g}^{-1} \mathbf{PQ}}.$$

Since $\mathbf{g}$ is symmetric its inverse is also symmetric. The SNR is thus

$$\rho = \begin{cases} \max_{\phi} P_{1i} Q_i (P_{1j} C_{jk} P_{k1})^{-1/2} & \text{if } \theta = \pi/2, \\ \max_{\theta,\phi} \sqrt{\mathbf{Q^T P^T} (\mathbf{PCP^T})^{-1} \mathbf{PQ}} & \text{otherwise.} \end{cases} \tag{A20}$$

Note that in performing the κ maximization we did not need to invoke the nonspinning assumption. Thus the argument of Eq. (A20) is valid for all systems; if there is spin, then further maximizations would need to be carried out over the spin components in addition to θ and ϕ.

APPENDIX B: ESTIMATING FALSE-ALARM PROBABILITY FROM A BANK OF TEMPLATES

The false-alarm probability of a template bank as a function of SNR depends on the size of the parameter space being searched over. The larger the parameter space, the greater the probability of getting a false alarm. Let us assume that every template in the bank is independent of each other. As described in Sec. II, in a search, intrinsic parameters are maximized over by selecting the template that yields the largest SNR. Due to this maximization, only one template can produce a trigger at any given time, making the probability of getting a trigger with some SNR from each template mutually exclusive. The false-alarm probability of the bank is thus

$$\mathcal{F}(\rho) = \sum_{k=1}^{N} \int_{\rho}^{\infty} f_B(\rho' | k) \mathrm{d}\rho',$$

where N is the number of templates in the bank and $f_B(\rho'|k)$ is the probability density function of the SNR of each template after maximization. Due to the bank

[17] Here repeated indices indicate sum over.

[18] We use $\langle\langle \cdot, \cdot \rangle\rangle$ to differentiate the inner product defined by $\mathbf{g}$ from the inner product defined in Eq. (4).

maximization $f_B(\rho|k)$ is given by the probability that the template produces an SNR equal to ρ times the probability that every other template produces an SNR less than ρ; thus

$$\mathcal{F}(\rho) = \sum_{k=1}^{N} \int_{\rho}^{\infty} f_P(\rho'|k) \prod_{l\neq k}^{N} \left[\int_0^{\rho'} f_P(\rho''|l) \mathrm{d}\rho'' \right] \mathrm{d}\rho' = \sum_{i=1}^{N} \int_{\rho}^{\infty} f_P(\rho'|k) \prod_{l\neq k}^{N} F_P(\rho'|l) \mathrm{d}\rho'. \quad \text{(B1)}$$

Here $f_P(\rho|k)$ is the SNR distribution in noise of the k^{th} template and $F_P(\rho|l)$ is the cumulative distribution function of the lth template.

In Gaussian noise, every dominant-mode template is χ distributed with 2 degrees of freedom. For a dominant-mode bank Eq. (B1) simplifies to

$$\mathcal{F}_{\mathrm{D}}(\rho) = 1 - (1 - e^{-\frac{\rho^2}{2}})^N. \quad \text{(B2)}$$

In our case, $N = 19800$ and $\rho = 8$; the probability that the dominant-mode bank produces a false alarm at SNR 8 is therefore $\approx 2.5 \times 10^{-10}$.

Note that Eq. (B2) approaches 1 as $N \to \infty$ for all $\rho > 0$. This is due to our assumption that the templates are independent of each other. We expect that as we increase the minimal match of the bank to 100% (which would require an infinite number of templates) the false-alarm probability would instead approach some limiting value for a given ρ. The minimal match of our template bank is 97%; assuming that templates are independent might therefore seem exceedingly naïve. To test this assumption we filtered the dominant mode template bank in 10000 realizations of noise. In each realization we selected the template with the best SNR to provide a measure of false-alarm probability as a function of SNR. We found good agreement between these results and Eq. (B2). Thus, despite a seemingly large overlap between neighboring templates, our assumption of independence appears to be approximately valid for the minimal match of our bank.

To model a search with subdominant modes we assume a bank with the same number of templates and with the same (M, q) coordinates as the dominant-mode bank. In such a search we would maximize ρ over θ, ϕ and κ for each template, then maximize over the entire bank. To find $\mathcal{F}(\rho)$ of this bank we need the probability density function of the SNR for each template in stationary Gaussian noise, $f_P(\rho|k)$. To find that we need an expression for the maximized SNR when subdominant modes are included. In Appendix A we analytically maximize ρ over κ to get Eq. (A20). This equation depends on the matrix $\mathbf{Q}$, the elements of which are the overlap between the template and the detector data [see Eq. (A18)]. In stationary Gaussian noise the Q_i are Gaussian random variables with variance $\sigma_i^2 = \sum_j C_{ij}$, where C_{ij} are the elements of the covariance matrix defined in Eq. (A15). To find $f_P(\rho|k)$ from this multivariate Gaussian distribution we need to maximize over θ and ϕ. This maximization is not trivial, however, and so we must find the SNR distribution numerically.

One way to find $f_P(\rho|k)$ is to generate many realizations of noise, filter it to get $\mathbf{Q}$, then perform the maximization in Eq. (A20) for each template. However, we expect the probability of getting $\rho \approx 8$ to be extremely small: the probability of getting 8 ± 0.1 from a χ distribution with 10 degrees of freedom (the upper limit of what we expect from a template with 5 modes) is order 10^{-9}. Getting an accurate measure of $f_P(\rho|k)$ around SNR 8 is thus computationally intractable using this "brute force" method. Instead, we follow a procedure similar to that used in Ref. [58] to find the probability density function.

To simulate a particular realization of $\mathbf{Q}$ we do not need to do any matched filtering; instead we draw a set $\mathbf{Z}$ of pseudorandom values from a Gaussian distribution with zero mean and unit variance. $\mathbf{Q}$ is then[19]

$$Q_i = [\sqrt{\mathbf{C}}]_{ij} Z_j.$$

We think of $\mathbf{Q}$ as being a vector in a ν dimensional space $\mathcal{S}$, where ν is equal to twice the number of modes; the relative size of each dimension is determined by the covariance matrix.

Now let $r = ||\mathbf{Z}||$ and $||\hat{\mathbf{Z}}|| = 1$ such that $\mathbf{Z} = r\hat{\mathbf{Z}}$. Define $\hat{\rho}$ to be the maximized SNR we obtain from a realization of $\hat{\mathbf{Q}} = \sqrt{\mathbf{C}}\hat{\mathbf{Z}}$. From Eq. (A20) we see that

$$\rho(\mathbf{Q}, k) = r\hat{\rho}(\hat{\mathbf{Q}}, k) \equiv r\hat{\rho}(\Omega, k). \quad \text{(B3)}$$

Here, Ω is the solid angle describing the direction of $\mathbf{Q}$ in $\mathcal{S}$, and we have made the dependence of the SNR on the intrinsic parameters of the kth template explicit. Since each element in $\mathbf{Z}$ is a Gaussian random variable with zero mean and unit variance, r—which is the quadrature sum of these variables—is χ distributed with ν degrees of freedom:

$$f_R(r|\nu) = \frac{r^{\nu-1} e^{-r^2/2}}{2^{\nu/2-1}\Gamma(\nu/2)}. \quad \text{(B4)}$$

The number of degrees of freedom is equal to the dimension of $\mathbf{Q}$, which is twice the number of modes. In our case, $\nu = 10$.

[19]Since $\mathbf{C}$ is positive-definite $\sqrt{\mathbf{C}}$ is real; we find it from the eigendecomposition of $\mathbf{C}$. Specifically, $\sqrt{\mathbf{C}} = \mathbf{T}\sqrt{\mathbf{\Lambda}}\mathbf{T}^{-1}$ where $\mathbf{T}$ is the matrix of the eigenvectors of $\mathbf{C}$ and $\mathbf{\Lambda}$ is the diagonal matrix formed from the eigenvalues.

Using the coordinate transformation given by Eq. (B3) we find

$$f_P(\rho|k,\Omega,\nu) = \frac{1}{\hat{\rho}(\Omega,k)} f_R\left(\frac{\rho}{\hat{\rho}(\Omega,k)}\middle|\nu\right). \quad \text{(B5)}$$

Marginalizing out Ω yields $f_P(\rho|k,\nu)$:

$$f_P(\rho|k,\nu) = \int \frac{1}{\hat{\rho}(\Omega,k)} f_R\left(\frac{\rho}{\hat{\rho}(\Omega,k)}\middle|\nu\right) d\Omega \Big/ \int d\Omega. \quad \text{(B6)}$$

We solve this via Monte Carlo integration. For each point in the Monte Carlo we generate a normalized random vector $\hat{\mathbf{Z}}$. We use Eq. (A20) to find $\hat{\rho}(\Omega)$ for this realization, with $\hat{\mathbf{Q}} = \sqrt{\mathbf{C}}\hat{\mathbf{Z}}$. We then find $f_P(\rho|k,\nu)$ with $\nu = 10$ for several different values of ρ, terminating the Monte Carlo when the error on $f_P(\rho|k)$ at $\rho = 9$ is less than 20%.

The top plot in Fig. 11 shows $f_P(\rho|k)$ for two different templates. We find that for $\rho \gtrapprox 7$, $f_P(\rho|k)$ approaches the χ distribution with noninteger number of degrees of freedom $f_X(\rho|\nu_k)$ for all templates. We therefore fit $f_X(\rho|\nu_k)$ to $f_P(\rho|k)$ between $\rho = 7$ and 9 by maximizing over ν_k. The bottom plot in Fig. 11 shows the best-fit ν_k ($\bar{\nu}_k$) for each template in the bank. If all of the modes were independent of each other $\bar{\nu}_k$ would be equal to 10 for all k. Instead we find that the largest $\bar{\nu}_k \approx 4.6$, which occurs at the largest mass ratio and total mass part of the bank. As the templates approach the equal mass line the number of degrees of freedom approaches 2. This is expected: as $q \to 1$, the subdominant modes become small relative to the dominant mode, and $f_P(\rho|k)$ reduces to a χ distribution with 2 degrees of freedom.

To solve Eq. (B1) we substitute $f_X(\rho|\bar{\nu}_k)$ and $F_X(\rho|\bar{\nu}_k)$ for $f_P(\rho|k)$ and $F_P(\rho|k)$, then numerically integrate for several different values of ρ. Inverting yields $\rho(\mathcal{F})$, which we solve for $\mathcal{F} = \mathcal{F}_{\mathrm{D}}(\rho = 8)$.

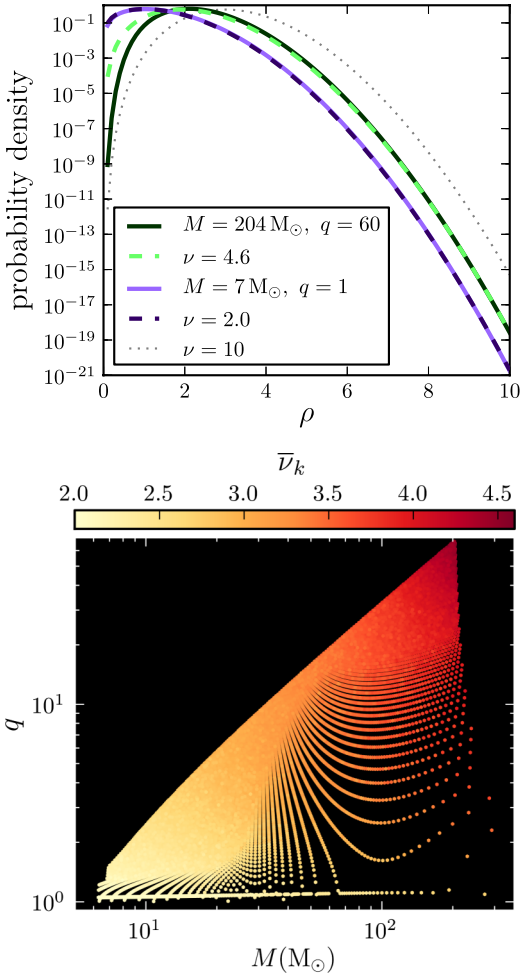

FIG. 11 (color online). SNR distribution in noise of two templates with subdominant modes [$f_P(\rho|k)$] versus SNR (top) and fitted number of degrees of freedom $\bar{\nu}_k$ for each template in total mass and mass-ratio q (bottom). The dashed lines in the top plot show a χ distribution with the fitted $\bar{\nu}_k$ to $f_P(\rho|k)$ of the templates shown. Fits were done between $\rho = 7$ and 9.

[1] G. M. Harry and the LIGO Scientific Collaboration, Classical Quantum Gravity **27**, 084006 (2010).

[2] T. Accadia *et al.* (Virgo Collaboration), Advanced Virgo technical design report, https://tds.ego-gw.it/itf/tds/file.php?callFile=VIR-0128A-12.pdf (2012).

[3] K. Somiya (KAGRA Collaboration), Classical Quantum Gravity **29**, 124007 (2012).

[4] IndiGO, http://www.gw-indigo.org/tiki-index.php.

[5] J. Abadie *et al.* (LIGO Scientific Collaboration, Virgo Collaboration), Classical Quantum Gravity **27**, 173001 (2010).

[6] J. Abadie *et al.* (LIGO Collaboration, Virgo Collaboration), Phys. Rev. D **85**, 082002 (2012).

[7] J. Aasi *et al.* (LIGO Scientific Collaboration, Virgo Collaboration), Phys. Rev. D **87**, 022002 (2013).

[8] J. Abadie *et al.* (LIGO Scientific Collaboration, Virgo Collaboration), Phys. Rev. D **85**, 122007 (2012).

[9] C. Pankow, S. Klimenko, G. Mitselmakher, I. Yakushin, G. Vedovato, M. Drago, R. A. Mercer, and P. Ajith, Classical Quantum Gravity **26**, 204004 (2009).

[10] B. Sathyaprakash and S. Dhurandhar, Phys. Rev. D **44**, 3819 (1991).

[11] R. Balasubramanian, B. S. Sathyaprakash, and S. V. Dhurandhar, Phys. Rev. D **53**, 3033 (1996).
[12] B. J. Owen, Phys. Rev. D **53**, 6749 (1996).
[13] Y. Pan, A. Buonanno, M. Boyle, L. T. Buchman, L. E. Kidder, H. P. Pfeiffer, and M. A. Scheel, Phys. Rev. D **84**, 124052 (2011).
[14] L. Pekowsky, J. Healy, D. Shoemaker, and P. Laguna, Phys. Rev. D **87**, 084008 (2013).
[15] D. A. Brown, P. Kumar, and A. H. Nitz, Phys. Rev. D **87**, 082004 (2013).
[16] D. McKechan, Ph.D. thesis, Cardiff University, 2011.
[17] A. Buonanno and T. Damour, Phys. Rev. D **59**, 084006 (1999).
[18] A. Buonanno and T. Damour, Phys. Rev. D **62**, 064015 (2000).
[19] A. Buonanno, Y. Pan, J. G. Baker, J. Centrella, B. J. Kelly, S. McWilliams, and J. van Meter, Phys. Rev. D **76**, 104049 (2007).
[20] T. Damour, A. Nagar, and S. Bernuzzi, Phys. Rev. D **87**, 084035 (2013).
[21] T. B. Littenberg, J. G. Baker, A. Buonanno, and B. J. Kelly, Phys. Rev. D **87**, 104003 (2013).
[22] L. T. Buchman, H. P. Pfeiffer, M. A. Scheel, and B. Szilagyi, Phys. Rev. D **86**, 084033 (2012).
[23] Y. Pan, A. Buonanno, A. Taracchini, M. Boyle, L. E. Kidder, A. H. Mroué, H. P. Pfeiffer, M. A. Scheel, B. Szilágyi, and A. Zenginoglu, Phys. Rev. D **89**, 061501 (2014).
[24] I. Hinder *et al.* (NRAR Collaboration, Perimeter Institute for Theoretical Physics), Classical Quantum Gravity **31**, 025012 (2013).
[25] B. Allen, Phys. Rev. D **71**, 062001 (2005).
[26] S. Babak *et al.*, Phys. Rev. D **87**, 024033 (2013).
[27] J. Abadie *et al.* (LIGO Scientific Collaboration, Virgo Collaboration), Phys. Rev. D **83**, 122005 (2011).
[28] M. C. Miller and E. J. M. Colbert, Int. J. Mod. Phys. D **13**, 1 (2004).
[29] D. Shoemaker (LIGO Collaboration), LIGO Report No. T0900288-v3, 2010.
[30] J. Aasi *et al.* (VIRGO Collaboration), Classical Quantum Gravity **29**, 155002 (2012).
[31] J. McIver (for LIGO Sceintific Collaboration and Virgo Collaboration), Classical Quantum Gravity **29**, 124010 (2012).
[32] J. Aasi *et al.* (LIGO Scientific Collaboration, Virgo Collaboration), Phys. Rev. D **88**, 062001 (2013).
[33] L. S. Finn and D. F. Chernoff, Phys. Rev. D **47**, 2198 (1993).
[34] B. F. Schutz and M. Tinto, Mon. Not. R. Astron. Soc. **224**, 131 (1987).
[35] B. Allen, W. G. Anderson, P. R. Brady, D. A. Brown, and J. D. E. Creighton, Phys. Rev. D **85**, 122006 (2012).
[36] T. Apostolatos, Phys. Rev. D **52**, 605 (1995).
[37] T. Damour, B. R. Iyer, and B. Sathyaprakash, Phys. Rev. D **57**, 885 (1998).
[38] P. R. Brady, J. D. E. Creighton, and A. G. Wiseman, Classical Quantum Gravity **21**, S1775 (2004).
[39] A. Agresti and B. A. Coull, Am. Stat. **52**, 119 (1998).
[40] LIGO Report No. T1200286-v3, 2012.
[41] J. M. Silverman and A. V. Filippenko, Astrophys. J. **678**, L17 (2008).
[42] P. A. Crowther, R. Barnard, S. Carpano, J. S. Clark, V. S. Dhillon, and A. M. T. Pollock, Mon. Not. R. Astron. Soc. **403**, L41 (2010).
[43] K. Belczynski, T. Bulik, C. L. Fryer, A. Ruiter, F. Valsecchi, J. S. Vink, and J. R. Hurley, Astrophys. J. **714**, 1217 (2010).
[44] M. Dominik, K. Belczynski, C. Fryer, D. Holz, E. Berti, T. Bulik, I. Mandel, and R. O'Shaughnessy, Astrophys. J. **759**, 52 (2012).
[45] M. Dominik, K. Belczynski, C. Fryer, D. E. Holz, E. Berti, T. Bulik, I. Mandel, and R. O'Shaughnessy, Astrophys. J. **779**, 72 (2013).
[46] M. C. Miller, Classical Quantum Gravity **26**, 094031 (2009).
[47] D. A. Brown, J. Brink, H. Fang, J. R. Gair, C. Li, G. Lovelace, I. Mandel, and K. S. Thorne, Phys. Rev. Lett. **99**, 201102 (2007).
[48] LSC Algorithm Library Suite, http://www.lsc-group.phys.uwm.edu/lal.
[49] T. Cokelaer, Phys. Rev. D **76**, 102004 (2007).
[50] B. J. Owen and B. S. Sathyaprakash, Phys. Rev. D **60**, 022002 (1999).
[51] S. Babak, R. Balasubramanian, D. Churches, T. Cokelaer, and B. S. Sathyaprakash, Classical Quantum Gravity **23**, 5477 (2006).
[52] D. Keppel, A. P. Lundgren, B. J. Owen, and H. Zhu, Phys. Rev. D **88**, 063002 (2013).
[53] P. Ajith, N. Fotopoulos, S. Privitera, A. Neunzert, and A. J. Weinstein, Phys. Rev. D **89**, 084041 (2014).
[54] A. Taracchini, Y. Pan, A. Buonanno, E. Barausse, M. Boyle, T. Chu, G. Lovelace, H. P. Pfeiffer, and M. A. Scheel, Phys. Rev. D **86**, 024011 (2012).
[55] P. Ajith *et al.*, Phys. Rev. Lett. **106**, 241101 (2011).
[56] L. Santamaria *et al.*, Phys. Rev. D **82**, 064016 (2010).
[57] D. A. Brown, I. Harry, A. Lundgren, and A. H. Nitz, Phys. Rev. D **86**, 084017 (2012).
[58] Y. Pan, A. Buonanno, Y. Chen, and M. Vallisneri, Phys. Rev. D **69**, 104017 (2004).